ELSEVIER

Coordination Chemistry Reviews
150 (1996) 185–220

COORDINATION CHEMISTRY REVIEWS

Chapter 7
Two-dimensional spectra and beyond

Contents

7.1. Introduction

Two-dimensional (2D) spectroscopy is a requirement to improve resolution every time there is a crowded region of the spectrum or when we want to measure small scalar coupling constants J_{IJ} between two nuclear spins I and J, and is always convenient because with a single experiment all the information which is obtained in a series of one-dimensional (1D) experiments can be obtained simultaneously. However, with the same experiment time the signal to noise ratio is decreased by at least a factor two. The parameters to obtain 2D spectra are nowadays well optimized for paramagnetic molecules, and useful information are obtained as long as the conditions dictated by the correlation time are not too severe. Sometimes care has to be taken to avoid that the fast return to thermal equilibrium of nuclei washes out the effects of the internuclear interactions that are sought through 2D spectroscopy.

2D NMR experiments are characterized by four time periods labeled preparation, evolution, mixing and detection (Fig. 7.1). The preparation period contains at least one pulse which alters the equilibrium population of at least one nucleus and generates some magnetization in the xy plane. The evolution period allows the magnetization to evolve in the xy plane according to the Larmor frequency of the nuclei which have experienced the preparation pulse(s). The evolution period is incremented in successive experiments and constitutes one of the two time domains

PII S0010-8545(96)01247-7

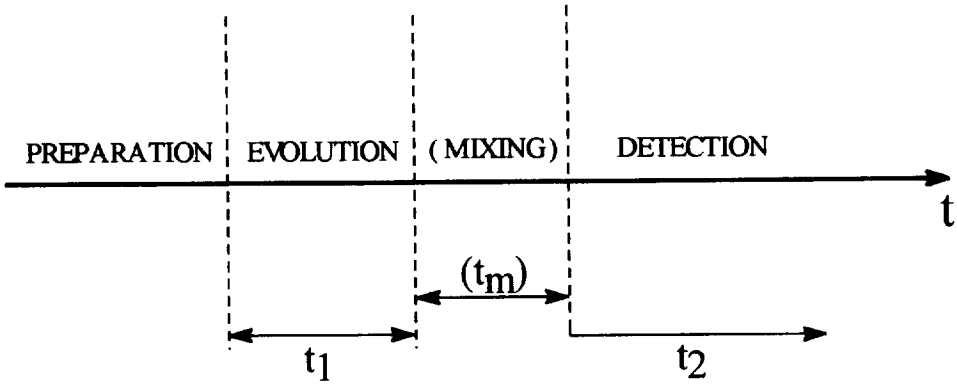

Fig. 7.1. General scheme of the time periods involved in 2D experiments.

(t_1) on which the Fourier transform is applied at the end of the 2D experiment. After this time interval a discontinuity is provided by either a pulse or the start of a spin lock sequence (see later), then the mixing follows. The mixing period t_m which may be lacking or may coincide with a pulse rather than a time period in some 2D experiments, allows for the transfer of magnetization or coherence (see later) between sets of spins which are connected by either dipolar or scalar coupling or by chemical exchange. At the end of the mixing period, which usually (but not always) has a constant duration throughout the experiment, the detection pulse provides the xy magnetization which is detected during the detection period as free induction decay. The time axis of the latter constitutes the second time domain (t_2) on which the Fourier transform is applied.

After Fourier transform in both dimensions, a 2D spectrum is obtained. The spectrum is characterized by two frequency axes, f_1 and f_2, which are related to t_1 and t_2 respectively, and represent the chemical shift scales of the experiment. Cross peaks represent the projections of signals which appear anytime a spin set affects another spin set either through dipolar coupling or scalar J_{IJ} coupling. The dipolar coupling allows magnetization transfer as has been shown in the NOE experiments. The J_{IJ} coupling is new to this book but it is quite familiar to all NMR researchers. It occurs through chemical bonds, i.e. two nuclei interact through the paired electrons of covalent bonds. Its magnitude, for instance for protons separated by three bonds ($^3J_{IJ}$), depends on the dihedral angle H_1–X–Y–H_2 in a way similar to that described in Section 2.4 for the contact hyperfine coupling. If this interaction is taken into account, after the perturbation of one or more nuclei the magnetization of two J_{IJ}-coupled nuclei evolves in a related way i.e. by obeying to the J_{IJ}-coupling requirement. This relationship allows what is called a *coherence transfer* to be performed. The meaning of coherence transfer is briefly recalled in Section 7.5. Magnetization transfer and coherence transfer may occur simultaneously depending on the system, and their separation is usually achieved through the so-called phase cycling.

2D experiments are devised in the assumption that the various times involved in the cycle of Fig. 7.1 (with the exception of t_m when present) are small with respect

to the nuclear relaxation times. When the latter are short for any reason, but in the present case because of the presence of unpaired electrons, the system of spins may have reached the equilibrium, or almost reached the equilibrium, before the detection pulse. Under these circumstances no memory is left for the state of the spins during the preceding steps. As a consequence, cross peaks may be decreased in intensity until below detectability. It is necessary, therefore, to match all the time intervals with the nuclear relaxation times, in order to detect the maximum possible cross peak intensities. The ideal case is that t_1 and t_2 are as short as possible, compatibly with spectral resolution, and in any case not much longer than T_2. Indeed, as during the acquisition time in 1D experiments, during t_1 and t_2 transverse magnetization is important. The latter decays with T_2. As far as the mixing time is concerned, it is again related to nuclear relaxation times in a fashion which will be described experiment by experiment (this consideration does not apply to COSY experiments, for which there is not a formal mixing time). Some gain can be obtained by a more rapid cycling because (1) the spin systems reach equilibrium quite fast, and (2) the overall time required by Fig. 7.1 is much shorter. The first 2D experiment on a system with T_1 in the range between 50 and 100 ms was an EXSY experiment (see later) which appeared in 1984 [1]. In 1985 the first NOESY appeared on a pseudotetrahedral nickel(II) complex [2]; in 1988 the first COSY appeared on a lanthanide complex [3,4]; in 1990 the first TOCSY experiment appeared on a five-coordinated nickel(II) complex [5]. Since then, the reports have been numerous, aiming also at the detection of cross peaks between signals with shorter and shorter T_1 values.

It has been mentioned in Section 6.3, and it was implicit all over Chapter 6, that a finite time is required to achieve selective saturation or inversion of a signal by a soft pulse, during which time magnetization starts to be exchanged, causing non-linearity of the response (see also Section 9.3). It should be stressed that this is not the case in all common 2D experiments based on non-selective pulses, which have durations of the order of microseconds instead of milliseconds, as required for selectivity. Selectivity in 2D experiments is intrinsic because of the double frequency labeling along f_1 and f_2.

We are now going to describe some 2D experiments performed on paramagnetic compounds (Fig. 7.2). We should stress that relatively few laboratories are engaged in making 2D spectroscopy suitable for the investigation of this type of compound. Therefore, whereas the literature is richer and richer in suitable sequences for the various cases in diamagnetic systems, few applications are devoted to paramagnetic systems. We have the feeling that a lot has still to be discovered in the NMR investigation of fast relaxing systems in order to reach the goal of solving the structure and describe the dynamics of paramagnetic molecules in a way similar to that described for diamagnetic molecules. We hope that the following examples will give a proper overview of the achievements which have represented a breakthrough in recent years.

7.2. The EXSY experiment

The 2D exchange spectroscopy (EXSY) is just an extension of the 1D saturation transfer experiment (Section 4.3.4). The simplest pulse sequence used to obtain EXSY

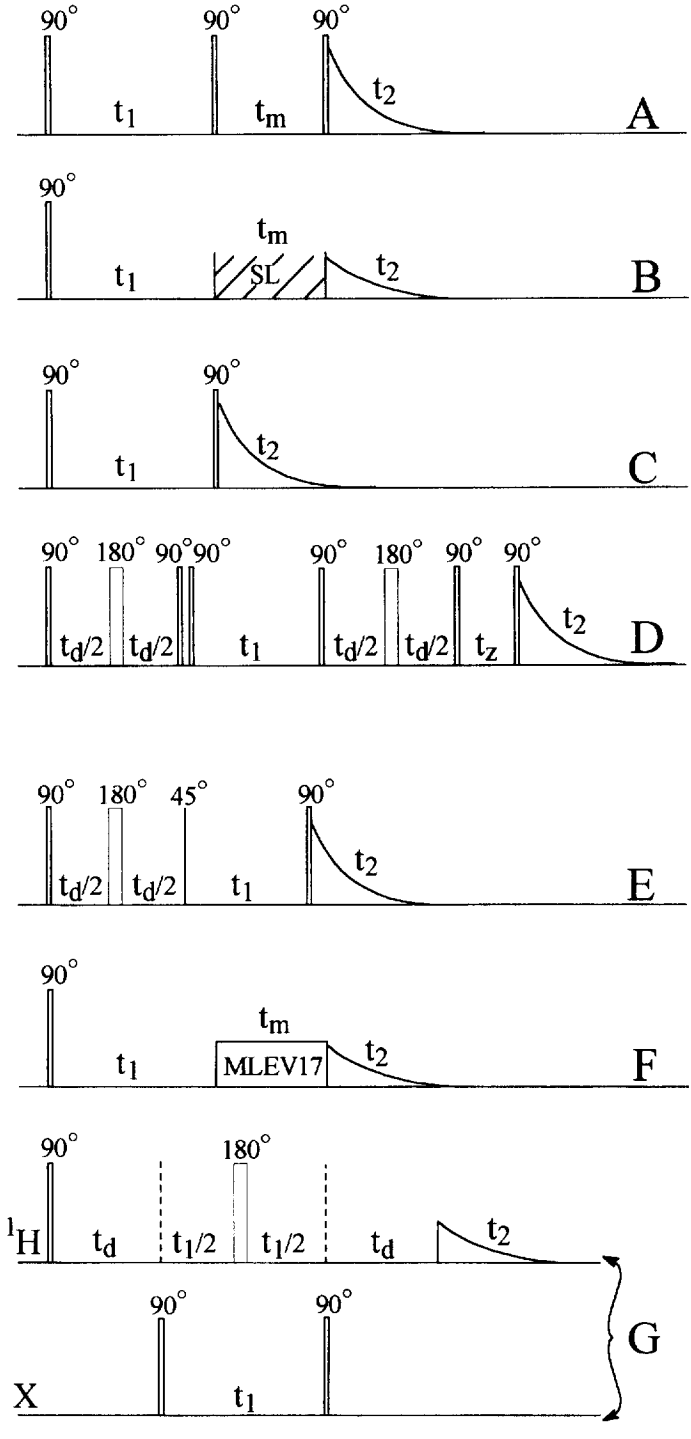
90°
90°
90°
t1
tm
t2
A
90°
tm
t1
SL
t2
B
90°
90°
t1
t2
C
90° 180° 90°90°
90° 180° 90° 90°
td/2 td/2
t1
td/2 td/2 tz
t2
D
90° 180° 45°
90°
td/2 td/2
t1
t2
E
90°
tm
t1
MLEV17
t2
F
90°
180°
1H
td
t1/2 t1/2
td
t2
90°
90°
X
t1
G

spectra is the NOESY sequence reported in Fig. 7.2(A). The first 90° pulse, constituting the preparation period of Fig. 7.1, tilts the z-magnetization along, e.g., the x axis in the rotating frame x' (Fig. 7.3); then the variable time interval t_1 is applied, during which the spins are labeled according to their frequency. This time must be short with respect to T_2, otherwise not enough in-plane magnetization remains to play with. Another 90° pulse is then applied which sends along $-z$ the component of the magnetization that is along x' at the end of the evolution period. At this point, during the fixed mixing time t_m, the nuclei of a given chemical species (e.g. A) transfer magnetization to the corresponding nuclei of the other species in chemical equilibrium (e.g. B), to an extent that is modulated by the difference in their z-components. After the time t_m, a 90° detection pulse is applied, which brings back to the xy plane

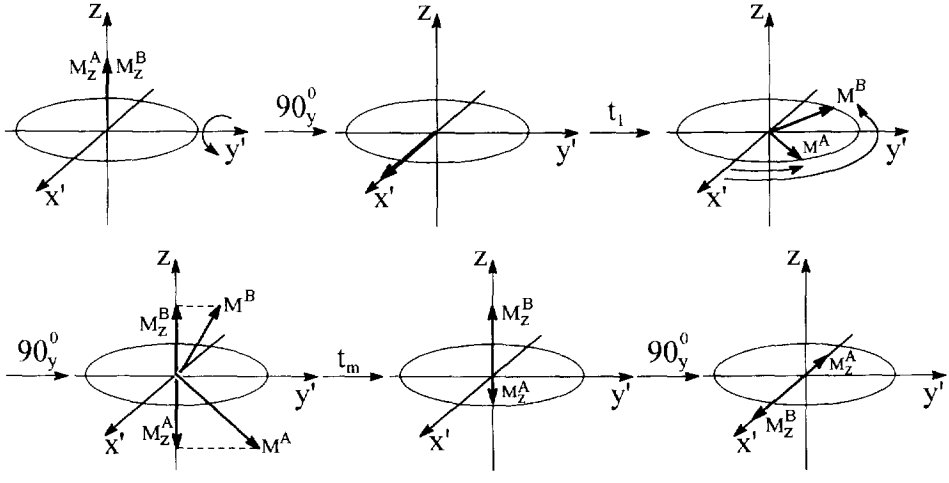

Fig. 7.3. Vector representation of an EXSY (or NOESY) experiment. The first 90° pulse along y' rotates the equilibrium magnetization of the A and B spins from the z axis to the x' axis. During t_1, the two transverse magnetizations precess in the $x'y'$ plane at their characteristic frequencies, and their x' (and y') components result periodically in and out of phase. The second 90° pulse tilts the two x' components along the z axis. During t_m, magnetization transfer occurs, to an extent that depends on how out of phase the two magnetization vectors were just before the second 90° pulse (i.e. depending on the value of t_1). The third pulse tilts the two z components, whose intensities have been altered during t_m in a t_1-dependent manner, along x'. Detection can then occur during t_2. In the presence of magnetization transfer, the intensity of (for example) the A signal detected during t_2 is thus modulated not only by its characteristic frequency but also by the frequency of the B signal. A cross peak is thus generated.

Fig. 7.2. Some of the most common 2D pulse sequences that can be employed using a proper choice of parameters to record 2D spectra of paramagnetic molecules: (A) NOESY, (B) ROESY, (C) COSY, (D) ISECR COSY, (E) zero-quantum (double quantum) COSY, (F) TOCSY, (G) HMQC. Sequences (A), (B) and (F) are also used to obtain EXSY spectra. SL indicates a soft spin-lock sequence, while MLEV17 indicates a train of spin-locking hard pulses that optimizes the development of J_{IJ} coupling. In the reverse heteronuclear experiment (G) the upper and lower levels refer to ^1H and heteronucleus respectively. The phase cycles are not indicated. For clarity of discussion, all initial pulses can be thought to be applied along the y' axis, in such a way that the magnetization after the first 90° pulse is always along x'.

the magnetization of the nuclei of the species in chemical equilibrium. The time t_m ideally should be much longer than the exchange time τ_M and much shorter than the T_1 values of the signals. If the exchange time is longer than T_1, then the best compromise is to set $t_m \simeq T_1$. The maximal information content in EXSY experiments is in the first t_1 and t_2 points. Generally, NMR spectroscopists apply a weighting function to the FID in order to optimize the response. Therefore, in this case we multiply the FID by a weighting function of cos- or $\cos^2$-type in order to give more "weight" to the first points.

We recall here that the phases of the pulses in Fig. 7.2(A) sequence, as well as of all other pulse sequences shown in Fig. 7.2 and described later in this chapter, must be properly cycled to achieve selection of the desired connectivities and suppression of artifacts and of other connectivities due to different types of interaction. The criteria to choose the appropriate phase cycling do not depend on the presence of a paramagnetic center in the molecule, and the reader should refer to the many publications on multidimensional NMR for details.

The first EXSY experiment on a paramagnetic system [1] described the chemical exchange between partially reduced species of a cytochrome c containing four hemes (Fig. 7.4). The electron exchange time could be estimated from the relative volumes of the cross peaks. The latter can be determined through numerical integration from the experimental signal intensities over a suitable area of the spectrum. Since the cross peak volume increases with the exchange rate, k_{-1} ($=\tau_M^{-1}$, as defined in Eq. (4.25)), and decreases with $(\rho^A + \rho^B)/2$ (A and B being the two species in chemical exchange), in analogy with Eq. (6.19), τ_M can in principle be determined from a single 2D experiment. However, if the aim is only that of measuring τ_M, it is more straightforward to perform a single steady state 1D experiment, as explained in Section 4.3.4. An EXSY experiment is shown in Fig. 7.5, relative to the complex praseodymium diethylenetriaminepentaacetate ($Pr(DTPA)^{2-}$) [3,4]. The complex undergoes chemical exchange between two conformational isomers. The T_1 values of the signals are around 30 ms.

EXSY experiments have the advantage of displaying cross peaks between many signals belonging to two or more complex species. In Fig. 7.6, the EXSY spectrum of a ferredoxin containing two Fe_4S_4 clusters is shown [6]. Here, the cross peaks connect the fully reduced species containing two $Fe_4S_4^+$ clusters with the intermediate species containing two "$Fe_4S_4^{1.5+}$" species and the oxidized species containing two $Fe_4S_4^{2+}$ species. The intermediate species actually contains one oxidized and one reduced cluster, which, however, are in very fast exchange so that, as far as NMR is concerned, only one intermediate species exists. It is noteworthy that we can detect as many as 20 signals of the intermediate species showing two cross peaks connecting them with those of the other two species. One of these patterns is exemplified in Fig. 7.6. Signal (b), arising from the $Fe_4S_4^{1.5+}$ species, is connected to both signal (a), belonging to the fully reduced species, and signal (c), belonging to the fully oxidized species. Signals (a) and (c) are also connected by a "two step" exchange cross peak, (a)–(c), whose nature is conceptually related to the spin diffusion mechanism described in Section 6.2.3.

EXSY cross peaks are also obtained in TOCSY experiments (see later) because

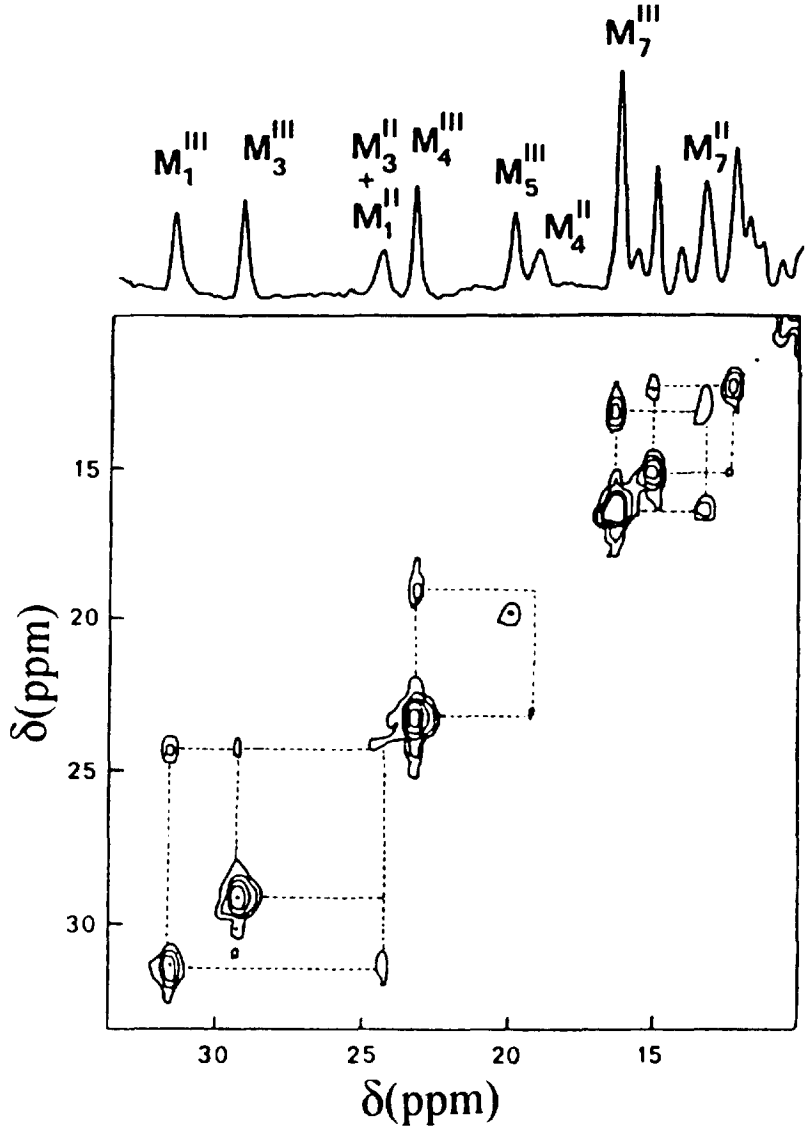

Fig. 7.4. The first EXSY experiment on a paramagnetic system [1]: the 300 MHz spectrum, taken with mixing time of 50 ms, shows species in chemical exchange belonging to two different redox states of a cytochrome c_3, a protein containing four low spin hemes. The signals marked M_1–M_7 represent various heme methyl groups. EXSY cross peaks are observed between M_i of two species containing two (II) or three (III) oxidized hemes respectively.

scalar interactions in the rotating frame are not separable from exchange interactions [7]. An EXSY experiment, performed using a TOCSY sequence (see later) is reported in Fig. 7.7 relative to the complex 5Cl–Ni–SAL–MeDPT [5]. This complex, as shown in Fig. 7.8, displays a chemical equilibrium in which the two salicylaldiminate

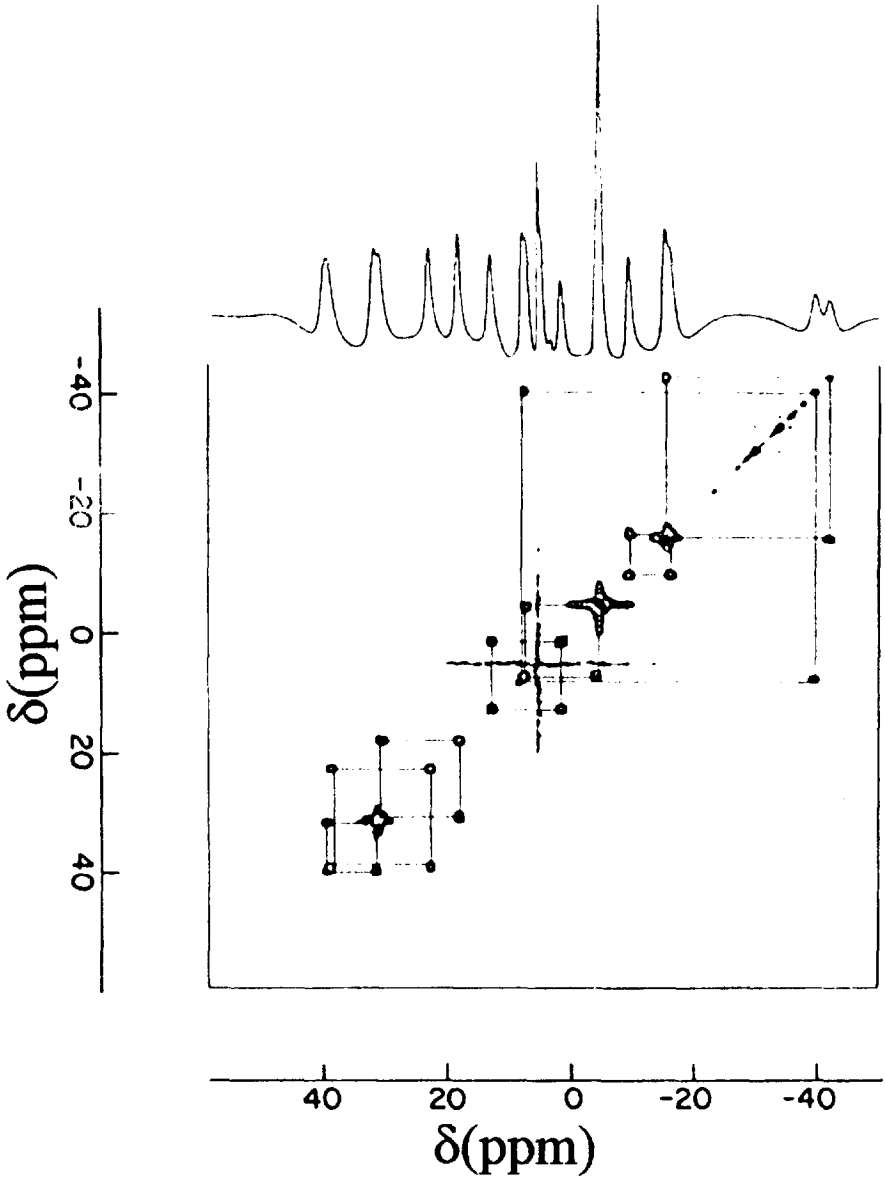

Fig. 7.5. 500 MHz EXSY spectrum of $Pr(DTPA)^{2-}$ recorded with the pulse sequence of Fig. 7.2(A) [4]. The spectrum demonstrates the presence of an equilibrium between two conformational isomers.

moieties exchange their non-equivalent positions [8]. It is interesting to learn that such complex interconversion occurs with times of the order of the spin lock time (20 ms) or shorter.

As EXSY cross peak intensities can be close to 100% in favorable cases, EXSY experiments can be performed with relative ease also on nuclei other than protons.

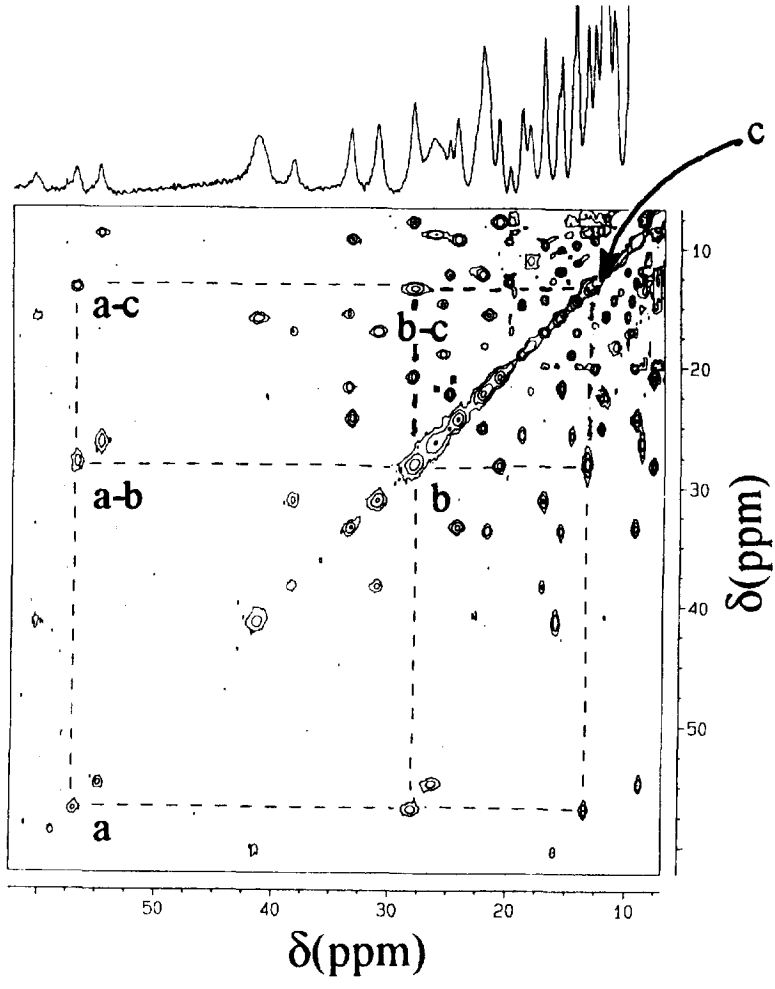

Fig. 7.6. 600 MHz EXSY spectrum of the intermediate reduction product of the $2Fe_4S_4$ ferredoxin from *C. pasteurianum*. Most signals of the intermediate species display cross peaks from both the fully reduced and the fully oxidized species. The sequence used is that in Fig. 7.2(A). $t_m = 5$ ms. A pattern belonging to a single signal exchanging among the three species ((a) fully reduced; (b) half reduced; (c) fully oxidized) is highlighted as an example.

EXSY experiments are sometimes performed with ROESY sequences (see Section 7.4).

7.3. The NOESY experiment

NOESY experiments deal with dipolar interactions between nuclei. Successful experiments are easily planned for nuclei with large magnetic moments like protons, or for heteronuclei when the dipole–dipole interaction is very strong.

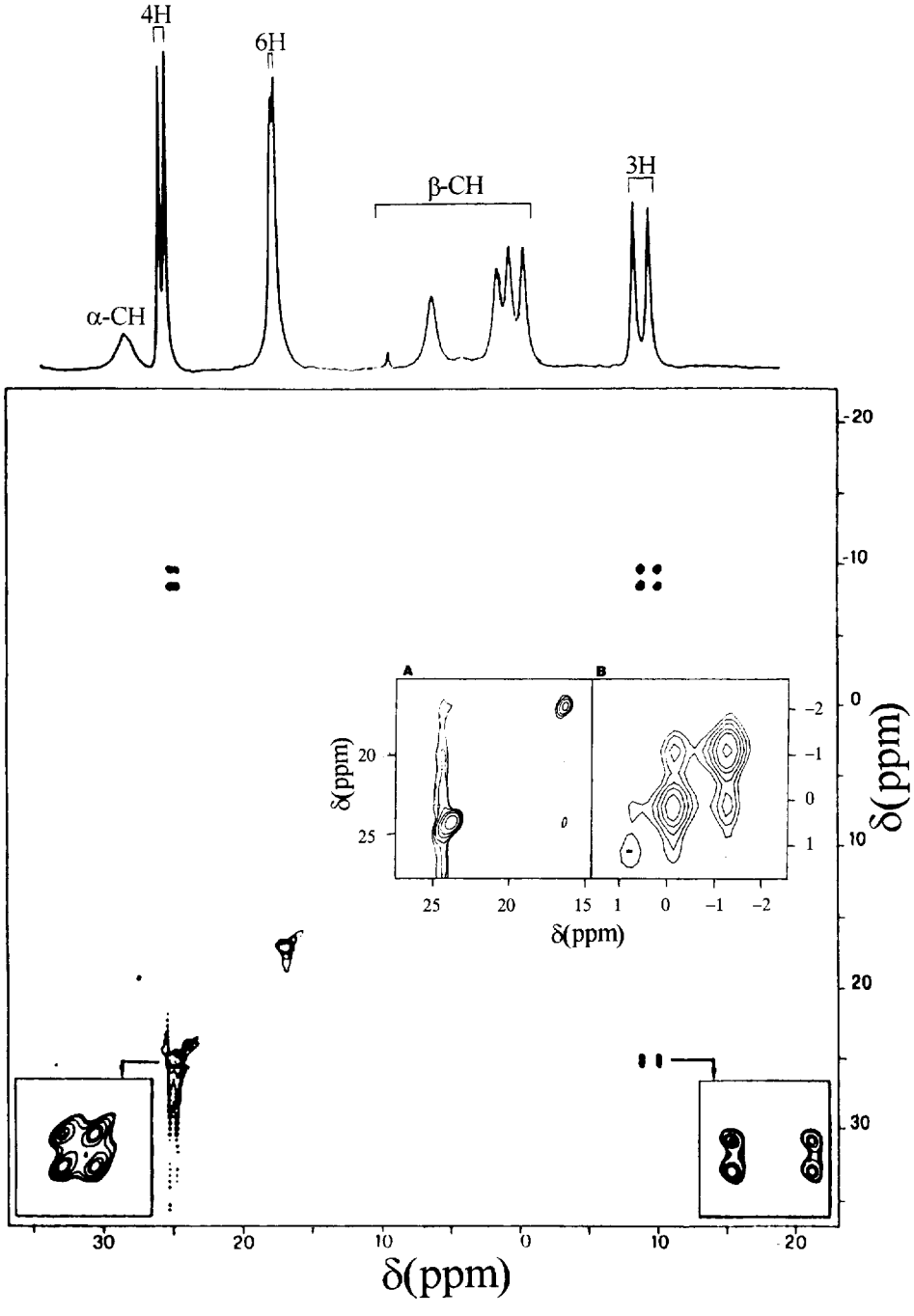

Fig. 7.7. TOCSY spectrum of the complex 5Cl–NiSAL–MeDPT (scheme in Fig. 7.8) showing exchange cross peaks between the two 4H ($T_1 = 5$ ms) and between the two 3H ($T_1 = 37$ ms) salicylaldiminate ring protons. The spin lock time was 20 ms.

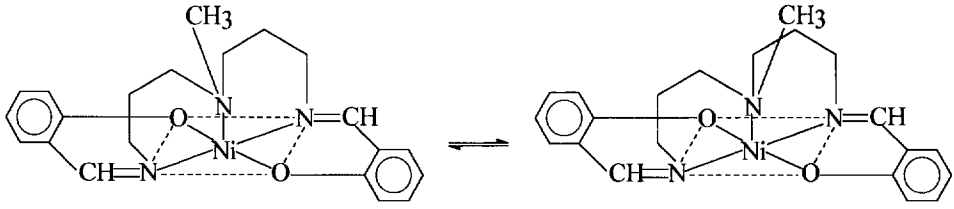

Fig. 7.8. Conformational equilibrium displayed by 5Cl–Ni–SAL–MeDPT. The two halves of the molecule are inequivalent owing to the CH_3 substituent on the apical nitrogen. The equilibrium involves two equivalent conformations differing in the chirality of the apical nitrogen [8].

The basic pulse sequence for the NOESY experiment is just that illustrated in Fig. 7.2(A). In the mixing period t_m magnetization transfer occurs between sets of nuclei I and J which are dipolarly coupled. After any given t_1 value and the second 90° pulse, the magnetization of the two sets of spins will be along z with different components. The situation is the same as that illustrated for the EXSY experiment of Fig. 7.3, if one substitutes the labels A and B for the two chemically exchanging sites with I and J for the two sets of nuclei. Just like in a transient NOE experiment, cross relaxation between the two sets of nuclei occurs. In order to predict the intensity of cross peaks, reference should be made to Fig. 6.8 and Eq. (6.19), provided it is considered that positive NOE corresponds to negative NOESY cross peaks and vice versa. This is not surprising if it is remembered that when the NOE is negative it has the same sign of the irradiated peak in the difference spectra. By referring to Fig. 6.8(B), and keeping in mind the reversal in sign, when τ_r is small, the NOESY cross peaks are small and negative (i.e. of opposite sign with respect to the diagonal peaks). With increasing τ_r they increase in absolute value and then decrease again until the zero value of the cross peak intensity is obtained. Then, the absolute intensities of positive cross peaks increase. This explains why NOESY experiments are best performed on macromolecules, unless very large concentrations can be reached. The best t_m is of the order of T_1. In the case in which the cross peak occurs between signals with sizably different T_1 values t_m can be optimized according to the following equation:

$$t_m^{max} = \frac{1}{2D} \ln\left(\frac{\rho - D}{\rho + D}\right) \tag{7.1}$$

where the symbols have the same meaning as in Eq. (6.19). A table is also provided for the reader's convenience (Table 7.1), which reports the best mixing time values t_m^{opt} for each combination of T_1^I and T_1^J (ρ_I^{-1} and ρ_J^{-1}) values for the pair [9]. Note that when the two T_1 values are very different, optimal t_m^{opt} is more than four times longer than the shorter T_1 value. As in EXSY experiments, the maximal information content is in the first t_1 and t_2 points. Again, the most used weighting functions are cos- or $\cos^2$-type.

NOESY experiments may sometimes be a hard task for small molecules, because in the fast motion limit cross relaxation is small and so is the NOE. In Table 7.2 the

Table 7.1
Optimal homonuclear NOESY mixing times t_m^{opt} for various T_1 (ρ^{-1}) values (ms) of the two spins I and J, calculated using Eq. (7.1). Cross peak intensities (%) for a $\sigma_{I(J)}$ value of $-1\,s^{-1}$ are shown in parentheses [9]

T_1^I	T_1^J							
	128	64	32	16	8	4	2	1
128	128	89.0	59.2	38.0	23.7	14.3	8.5	4.9
	(4.72)	(3.20)	(2.02)	(1.19)	(0.67)	(0.36)	(0.19)	(0.10)
64	89.0	64.1	44.4	29.6	19.0	11.8	7.2	4.2
	(3.20)	(2.36)	(1.60)	(1.01)	(0.59)	(0.33)	(0.18)	(0.09)
32	59.2	44.4	32.0	22.2	14.8	9.5	5.9	3.6
	(2.02)	(1.60)	(1.18)	(0.80)	(0.50)	(0.30)	(0.17)	(0.09)
16	38.0	29.6	22.2	16.0	11.1	7.4	4.8	3.0
	(1.19)	(1.01)	(0.80)	(0.59)	(0.40)	(0.25)	(0.15)	(0.08)
8	23.7	19.0	14.8	11.1	8.0	5.5	3.7	2.4
	(0.67)	(0.59)	(0.50)	(0.40)	(0.29)	(0.20)	(0.13)	(0.07)
4	14.3	11.8	9.5	7.4	5.5	4.0	2.8	1.8
	(0.36)	(0.33)	(0.30)	(0.25)	(0.20)	(0.15)	(0.10)	(0.06)
2	8.5	7.2	5.9	4.8	3.7	2.8	2.0	1.4
	(0.19)	(0.18)	(0.17)	(0.15)	(0.13)	(0.10)	(0.07)	(0.05)
1	4.9	4.2	3.6	3.0	2.4	1.8	1.4	1.0
	(0.10)	(0.09)	(0.09)	(0.08)	(0.07)	(0.06)	(0.05)	(0.04)

calculated ^1H–^1H maximal NOESY intensities are reported for a range of τ_r values and R_{1M} values (taken equal for the two spins). From the τ_r values the corresponding molecular weights are calculated through the Stokes–Einstein equation (Eq. (3.7)) for $\eta = 1$. The mixing time is always equal to ρ_I ($= \rho_{I(J)} + R_{1M}$) to maximize the effect. The NOEs are reported for two magnetic fields and for two proton–proton distances of 1.8 and 3.0 Å. The purpose of this table is to show under which circumstance NOESY spectra of paramagnetic molecules can be attempted. The crossing point between fast and slow motion regimes occurs at $MW \approx 800$ at 600 MHz and at $MW \approx 2500$ at 200 MHz. The maximal intensities in the fast motion regime are always small in absolute value and therefore the observability of cross peaks is predictable but critical. The researcher dealing with low molecular weight compounds may either use low fields or increase τ_r by increasing solvent viscosity and use the highest possible field.

As discussed in Section 6.2.3, spin diffusion is not a problem in small complexes. In macromolecules, the problems are negligible when the nuclear R_{1M} values are

Fig. 7.9. NOESY spectra of the oxidized form of 2(Fe_4S_4) ferredoxin from *C. pasteurianum* taken using mixing times of 20 (A), 10 (B) and 5 (C) ms. Signals (a)–(h) belong to β-CH protons of cluster-coordinated cysteines and cross peaks 1–8 connect them to their geminal partners, which lie in the diamagnetic region of the spectrum. The other cross peaks arise from α-CH protons of the cysteines and from other nearby residues. The cross peaks between the fastest relaxing signals (β-CH protons with their geminal partners) are maximal at the shortest mixing time, whereas those between the former and more slowly relaxing signals increase at longer mixing times [10].

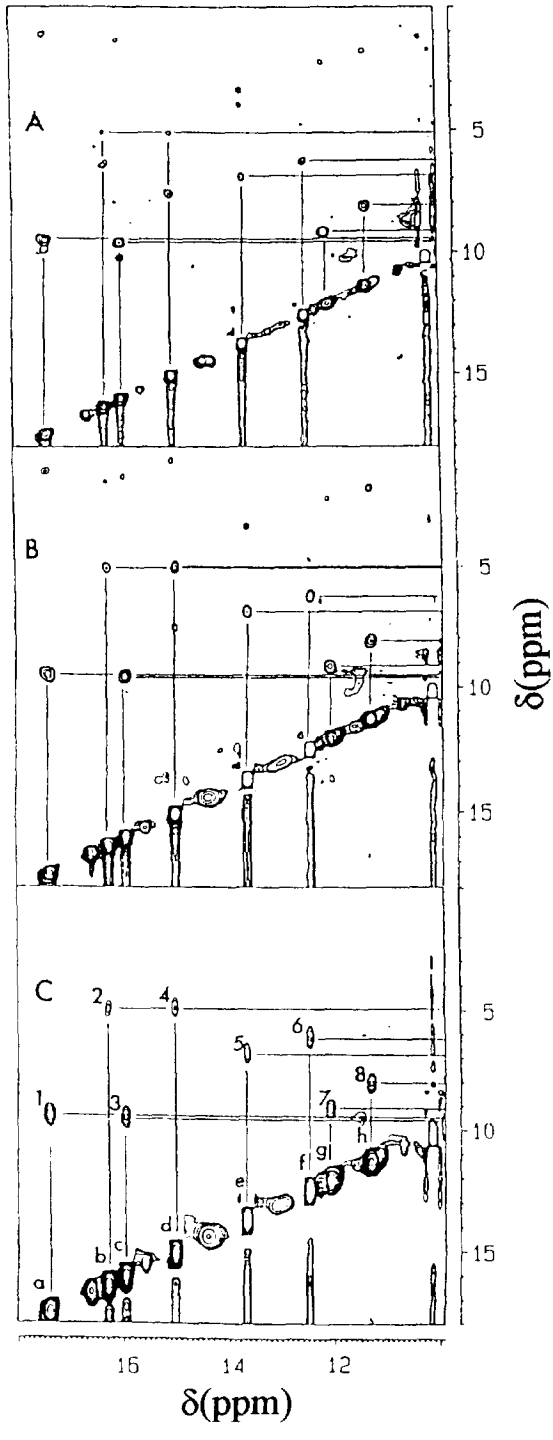
A
B
C
5
10
15
δ(ppm)
16
14
12
δ(ppm)

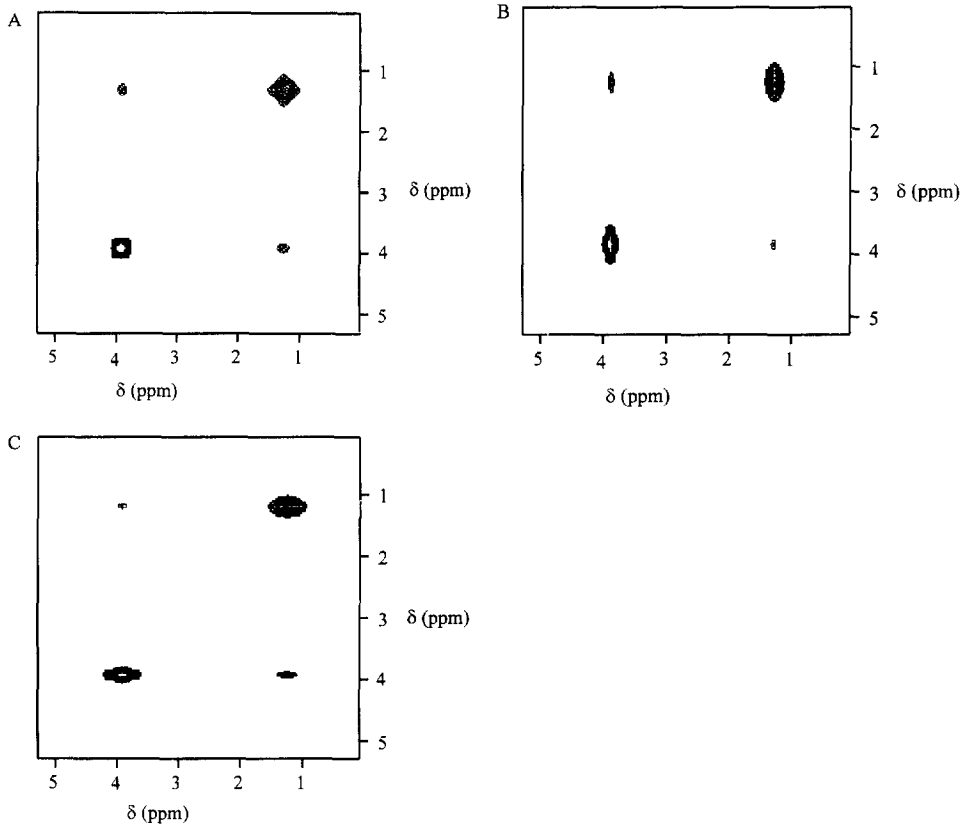

Fig. 7.10. Computer-simulated NOESY cross peaks between signals with different T_2 values. Conditions: $\rho_1^I = \rho_1^J = 40\ s^{-1}$; $\rho_2^I = 50\ s^{-1}$; $\rho_2^J = 200\ s^{-1}$; $\sigma_{IJ} = 5\ s^{-1}$. (A) $t_1^{max} = t_2^{max} = 100\ s^{-1}$; (B) $t_1^{max} = T_2^I$, $t_2^{max} = T_2^J$; (C) $t_1^{max} = T_2^J$, $t_2^{max} = T_2^I$. Note that the upper left cross peak has maximal intensity in case (B), the lower right cross peak has maximal intensity in case (C), whereas in case (A) the two intensities are equal and intermediate between the larger and the smaller of cases (B) and (C). For simplicity, $t_m = T_1^I = T_1^J$ has been taken. A $\cos^2$ weighting function has been applied.

much larger than cross relaxation. Such problems become increasingly significant when the R_{1M} values get smaller. Under these circumstances it may be useful to perform the NOESY experiments at different mixing times. At short mixing times (short relative to T_1) only primary NOEs are detected whose intensities are proportional to σ. At increasing mixing time, the build up of these signals can be followed and new cross peaks may appear. In macromolecular systems the best conditions for measuring NOESY cross peaks are met, because τ_r is long (see Table 7.2). In Fig. 7.9 the NOESY spectrum of an Fe_4S_4 protein of MW 6000 is shown where cross peaks are apparent between signals with T_1 values of a few milliseconds [10]. With mixing time of the order of few milliseconds NOESY cross peaks are observed between signals with short T_1, whereas NOESY cross peaks are observed between signals with longer T_1 values if longer mixing times are used. The observation of

Table 7.2
Calculated maximal intensities of NOESY cross peaks (%)[a] for various values of τ_r and R^I_{1M} (= R^J_{1M}). For each τ_r and R^I_{1M} value two NOEs are calculated for interproton distances of 1.8 and 3.0 Å and for nuclear Larmor frequencies ν_0 of 200 and 600 MHz

τ_r (s) [MW(Da)]	r_{IJ} (Å)	R^I_{1M}(s^{-1})																	
		1		2		4		8		16		32		64		128		256	
		ν_0 (MHz)		ν_0 (MHz)		ν_0 (MHz)		ν_0 (MHz)		ν_0 (MHz)		ν_0 (MHz)		ν_0 (MHz)		ν_0 (MHz)		ν_0 (MHz)	
		200	600	200	600	200	600	200	600	200	600	200	600	200	600	200	600	200	600
10^{-11}	1.8	−2.640	−2.626	1.421	−1.413	−0.739	−0.735	−0.377	−0.375	−0.190	−0.189	−0.096	−0.095	−0.048	−0.048	−0.024	−0.024	−0.012	−0.012
[25]	3.0	−0.143	−0.142	0.072	−0.071	−0.036	−0.036	−0.018	−0.018	−0.009	−0.009	−0.004	−0.004	−0.002	−0.002	−0.001	−0.001	−0.001	−0.001
$10^{-10.5}$	1.8	−6.366	−6.089	−3.835	−3.647	−2.138	−2.025	−1.135	−1.072	−0.585	−0.552	−0.297	−0.280	−0.150	−0.141	−0.075	−0.071	−0.038	−0.036
[80]	3.0	−0.440	−0.416	−0.223	−0.210	−0.112	−0.106	−0.056	−0.053	−0.028	−0.027	−0.014	−0.013	−0.007	−0.007	−0.004	−0.003	−0.002	−0.002
10^{-10}	1.8	−11.236	−8.248	−8.045	−5.587	−5.141	−3.400	−2.989	−1.909	−1.628	−1.017	−0.852	−0.526	−0.436	−0.267	−0.221	−0.135	−0.111	−0.068
[250]	3.0	−1.244	−0.772	−0.644	−0.396	−0.328	−0.200	−0.165	−0.101	−0.083	−0.051	−0.042	−0.025	−0.021	−0.013	−0.010	−0.006	−0.005	−0.003
$10^{-9.5}$	1.8	−11.920	0.890	−9.679	0.616	−7.045	0.381	−4.568	0.216	−2.685	0.116	−1.472	0.060	−0.774	0.031	−0.397	0.015	−0.201	0.008
[800]	3.0	−2.098	0.088	−1.127	0.045	−0.585	0.023	−0.298	0.012	−0.151	0.006	−0.076	0.003	−0.038	0.001	−0.019	0.001	−0.010	0.000
10^{-9}	1.8	2.343	19.647	1.934	14.379	1.434	9.406	0.945	5.581	0.562	3.084	0.310	1.629	0.164	0.838	0.084	0.425	0.043	0.214
[2500]	3.0	0.441	2.366	0.238	1.233	0.124	0.630	0.063	0.319	0.032	0.160	0.016	0.080	0.008	0.040	0.004	0.020	0.002	0.010
$10^{-8.5}$	1.8	27.084	33.735	23.302	28.378	18.275	21.644	12.831	14.784	8.080	9.111	4.657	5.176	2.525	2.782	1.319	1.446	0.674	0.738
[8000]	3.0	6.464	7.238	3.619	4.005	1.926	2.118	0.996	1.091	0.506	0.554	0.255	0.279	0.128	0.140	0.064	0.070	0.032	0.035
10^{-8}	1.8	38.951	39.972	36.394	37.299	32.208	32.938	26.264	26.779	19.296	19.610	12.702	12.872	7.591	7.677	4.220	4.262	2.238	2.259
[25000]	3.0	16.387	16.633	10.331	10.459	5.969	6.033	3.244	3.275	1.697	1.712	0.869	0.876	0.440	0.443	0.221	0.223	0.111	0.112
$10^{-7.5}$	1.8	42.060	42.175	41.073	41.183	39.238	39.339	36.040	36.127	31.041	31.109	24.401	24.446	17.209	17.235	10.909	10.923	6.332	6.339
[80000]	3.0	28.398	28.455	21.347	21.383	14.373	14.393	8.754	8.764	4.932	4.937	2.638	2.640	1.367	1.368	0.696	0.697	0.352	0.352
10^{-7}	1.8	42.884	42.896	42.554	42.565	41.909	41.920	40.678	40.689	38.432	38.442	34.639	34.647	28.998	29.004	21.987	21.991	14.933	14.935
[250000]	3.0	37.050	37.059	32.481	32.488	26.145	26.150	18.928	18.931	12.291	12.293	7.268	7.269	4.012	4.012	2.118	2.119	1.090	1.090

[a] The largest theoretical cross peak intensity for a NOESY experiment is 50%, at variance with a transient NOE experiment (Section 6.4). To predict the maximal values for transient NOE experiments the values of this table should be multiplied by two and the sign should be reversed. Cf. also Table 6.1 for steady state NOE experiments.

cross peaks between fast relaxing and slow relaxing signals can be accomplished with mixing times appropriately chosen according to Table 7.1. The difference in T_2, which often parallels the difference in T_1, provides elliptical cross peaks (as shown in Fig. 7.10(A)). The maximal value of t_1 (t_1^{max}) is best chosen to be equal to or less than one of the two T_2 values, and the maximal value of t_2 (t_2^{max}) to be equal to or less than that of the other. Under these circumstances, one of the two cross peaks on one side of the diagonal is enhanced whereas the other is sacrificed (Figs. 7.10(B) and 7.10(C)). The difficulty, which is a limit of the technique, is that it is often not possible to see in the same 2D map cross peaks arising from signals with strongly different T_1 and T_2 values. If reference is made to the system of Fig. 7.9 we see that only some cross peaks are evident between β-CH_2 protons of cysteines and between β-CH_2 and α-CH protons. If some other cross peaks are observed between β-CH_2 and other more diamagnetic protons, then cross peaks between the latter and diamagnetic protons are absolutely missing. When we increase the mixing time in order to detect the latter part, the cross peaks with the β-CH_2 are sizably reduced in intensity and will be eventually lost. The procedure used up to now is that of firmly recognizing signals farther from the paramagnetic center to which the β-CH protons are dipolarly connected (mostly through 1D NOE), and then try to relate them to known dipolar patterns observed in the diamagnetic region of NOESY spectra recorded with longer t_m, t_1^{max} and t_2^{max}.

From comparison of Table 7.2 with Table 6.2 (or of Eq. (6.20) with Eq. (6.10), i.e. of transient NOE or NOESY vs. steady state NOE intensities, it appears that the latter are superior under any circumstance. This superiority is striking if the intrinsic asymmetry of the steady state NOE with respect to the symmetry of transient NOE and NOESY experiments (Section 6.4) can be exploited, as in the case of irradiation of fast relaxing nuclei to detect NOE to slow relaxing nuclei. Of course, NOE experiments are advantageous over NOESY experiments if one is looking for dipolar connectivities from only a few specific signals.

Sometimes the shifts of a few signals are so large that it is inconvenient to include them into the spectral window because this will either decrease the resolution or, if resolution is maintained by increasing the data points in the two dimensions, cause cumbersome spectral manipulations. Then, it may be convenient to use a smaller spectral width and allow the excluded signals to appear as folded images, or "ghost" signals. This can be easily accomplished in the f_1 dimension by increasing the time increment in t_1 between one experiment and the next [11]. It can also be accomplished in the f_2 dimension by likewise increasing the dwell time, provided the filter width is chosen large enough to include all the signals. Ghost signals give "ghost" cross peaks. An example of this is illustrated in Fig. 7.11(A), showing the 600 MHz NOESY spectrum of the four-cobalt cluster of Co_7MT, with MT indicating the protein metallothionein ($MW \approx 6000$) [12].

Sometimes the signals are outside the maximal spectral width allowed by the ADC of the instrument. In this case the folded spectrum is a necessity. Another possibility is that of using an ADC with smaller dynamic range (e.g. 12 bit instead of 16 bit at the present level of technology) but larger spectral window (e.g. ca. 5–10 MHz instead of ca. 100–200 kHz). Fig. 7.11(B) shows the 600 MHz NOESY spectrum of the above

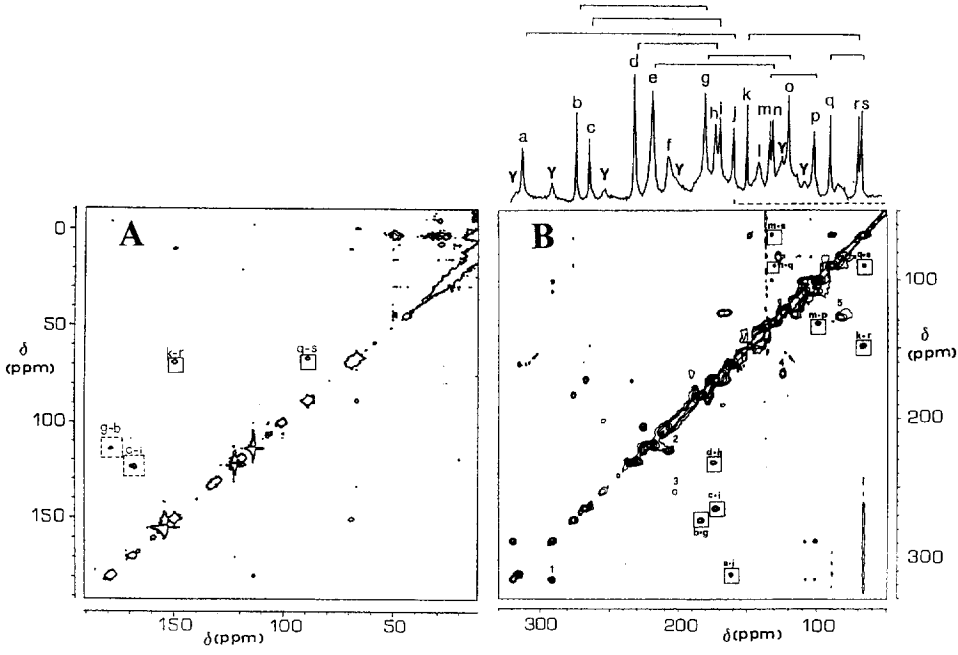

Fig. 7.11. 600 MHz NOESY spectra of the four-cobalt cluster of cobalt-substituted metallothionein. The spectra have been recorded with $t_m = 7$ ms using a specially built probe featuring a 90° pulse of 3.7 μs. (A) Spectrum obtained with a 125 kHz 16 bit ADC by folding the spectrum in both dimensions; cross peaks *g–b* and *c–i* are folded. (B) Spectrum recorded using a fast ADC over a 250 kHz spectral width. The nine observed connectivities between geminal protons of cobalt-coordinated cysteine β-CH_2 are summarized in the inset. Cross peaks marked with numbers are EXSY cross peaks to a minor species labeled Y in the inset [12].

protein complex [12] covering a spectral width of 250 kHz, recorded with a 12 bit ADC. At least nine out of the 11 expected cross peaks between geminal protons of cysteine β-CH_2 (see inset of Fig. 7.11) are observed. Some of the signals giving rise to cross peaks have T_1 values as short as 1 ms.

Of course, these considerations regarding the folded spectra and decreased dynamic range of the ADC hold for any kind of 2D spectroscopy. We have mentioned them here because such problems happen to have been afforded in the NMR literature on paramagnetic compounds in connection with NOESY spectra.

7.4. The ROESY experiment

The 2D ROE or ROESY experiment is a spin locked 2D experiment (Fig. 7.2(B)). After an initial 90° pulse and the variable evolution period t_1, a low power or "soft" spin lock sequence (SL) is applied for a time t_m during which magnetization transfer in the rotating frame occurs. The SL is often applied off resonance to avoid generation of TOCSY cross peaks (see Section 7.6). Then, acquisition is performed, using weighting functions of cos or $\cos^2$ type. As shown in Fig. 6.10, the ROE is always

positive, so that ROESY cross peaks are always negative (i.e. opposite to the diagonal) independently of the magnitude of τ_r. ROESY experiments are thus most useful for relatively small molecules where NOESY cross peak intensities may be close to zero ($\omega_I \tau_r \approx 1$, see Section 6.5). As in NOESY, magnetization transfer occurs through dipolar coupling, and applications are limited to protons. A comparison between a NOESY and a ROESY spectrum of a metalloprotein containing four heme groups is reported in Fig. 7.12 [13].

It should be noted that NOESY and ROESY pulse sequences also provide EXSY spectra, and therefore EXSY cross peaks may appear simultaneously in the 2D

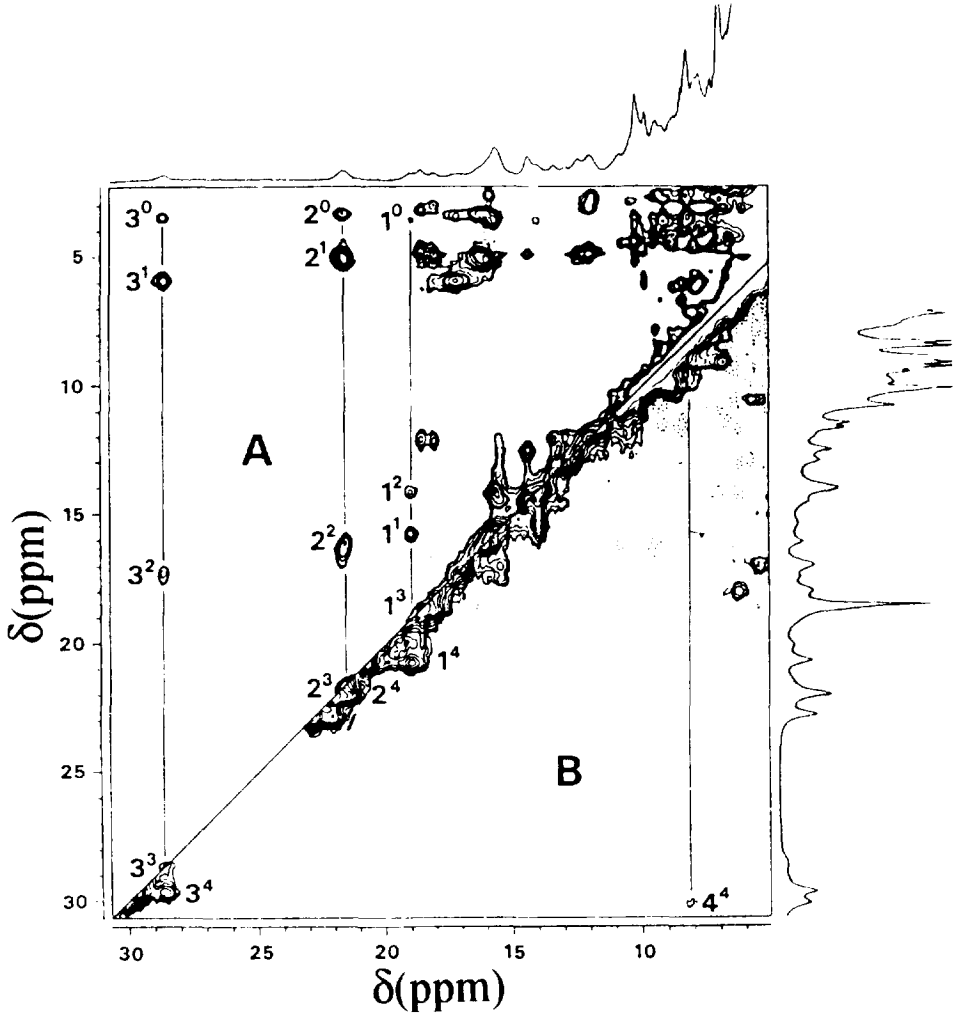

Fig. 7.12. NOESY (A) and ROESY (B) spectrum of a four heme cytochrome. The exchange cross peaks in the two spectra have the same sign and give information on different interactions [13].

NOESY and ROESY spectra. EXSY cross peaks are always positive in both types of experiment, whereas dipolar cross peaks are negative in EXSY spectra independently of molecular weight and in NOESY spectra of small molecules. Therefore, in macromolecules the sign for NOESY and EXSY cross peaks is the same, and the two phenomena cannot be distinguished in NOESY experiments. In contrast, ROESY cross peaks have different sign from EXSY cross peaks and can be distinguished and even plotted selectively in ROESY experiments. These considerations are summarized in Table 7.3 for the reader's convenience.

The problem with spin locking experiments, which is common to TOCSY (see Section 7.6), is that spin locking of signals over a wide range requires sizable r.f. power, which is sometimes not available or, if available, cannot be delivered to the sample because heat cannot be dissipated fast enough. However, the mixing times used for paramagnetic systems are generally shorter than for diamagnetic systems, so that the total energy (higher power × shorter time) delivered to the sample may be of the same order of that used in diamagnetic systems. Even so, temperature and lock instabilities may arise. This problem, together with the intrinsic higher sensitivity of NOESY with respect to ROESY makes the former a more common investigation tool. In the problem illustrated in Fig. 7.12 the spectral width is relatively small.

As an example of a system in the fast motion regime, a portion of the ROESY spectrum of a small lanthanide diporphyrin complex is shown in Fig. 7.13, together with portions of the NOESY and TOCSY spectra [14]. The subspectra refer to phenyl rings attached in the meso position to one of the two coordinated porphyrins (Fig. 7.13, inset). The flip rate of the rings is slow on the chemical shift scale but fast on the relaxation time scale. Therefore, separate signals are observed for the exo and endo ortho and meta ring protons. Strong and positive (Table 7.3) EXSY cross peaks are apparent in ROESY and NOESY spectra (as well as in the TOCSY spectrum, see Section 7.6), whereas all dipole–dipole cross peaks are negative in the ROESY and NOESY spectra. In the latter, only one dipole–dipole cross peak is observed, on account of the rotational correlation time of the system being close to the null point for the NOE interaction [14] (see also Sections 6.2 and 6.5).

7.5. The COSY experiment

The COSY experiment is the most familiar to 2D NMR spectroscopists. The cross peaks connect protons which are coupled by scalar interactions. Under these condi-

Table 7.3
Signs of 1D difference spectra or 2D cross peaks arising from dipole–dipole or chemical exchange interactions in fast (FM) and slow (SM) motion regimes[a]

Experiment	1D NOE		NOESY		1D ROE		ROESY	
Motion regime	FM	SM	FM	SM	FM	SM	FM	SM
Dipole–dipole	+	−	−	+	+	+	−	−
Chemical exchange	−	−	+	+	−	−	+	+

[a] Signs of 1D experiments are referred to a negative irradiated signal; signs of 2D experiments are referred to a positive diagonal peak.

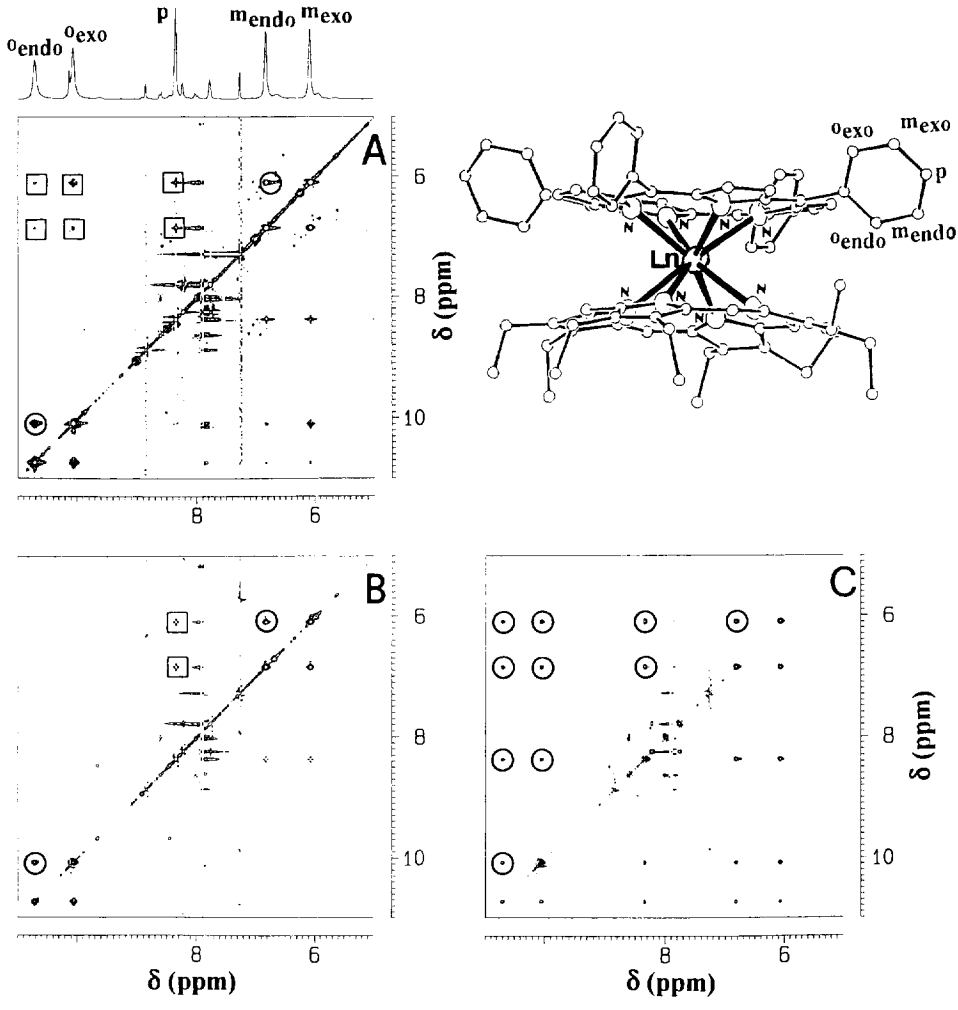

Fig. 7.13. ROESY (A), NOESY (B) and TOCSY (C) cross peaks observed in the phenyl ring 2D pattern of the complex shown in the inset (Ln = Yb^{3+}). Negative cross peaks are highlighted by squares, and positive cross peaks by circles [14].

tions each signal of a two-spin system I–J is split into two components, whose separation in frequency is determined by the scalar coupling constant J_{IJ}. The simplest COSY pulse sequence is that reported in Fig. 7.2(C). There is an initial 90° pulse followed by the evolution time t_1, during which antiphase magnetization of the scalar-coupled spins builds up. The concept of antiphase magnetization is recalled in Fig. 7.14. The magnetization of the two components of (for example) the I doublet, rotates in the xy plane at different frequency. In a frame rotating at the frequency of the center of the doublet, the two components will rotate in opposite directions with frequency $\pm J_{IJ}/2$. The two in-plane components arise from I spins whose J

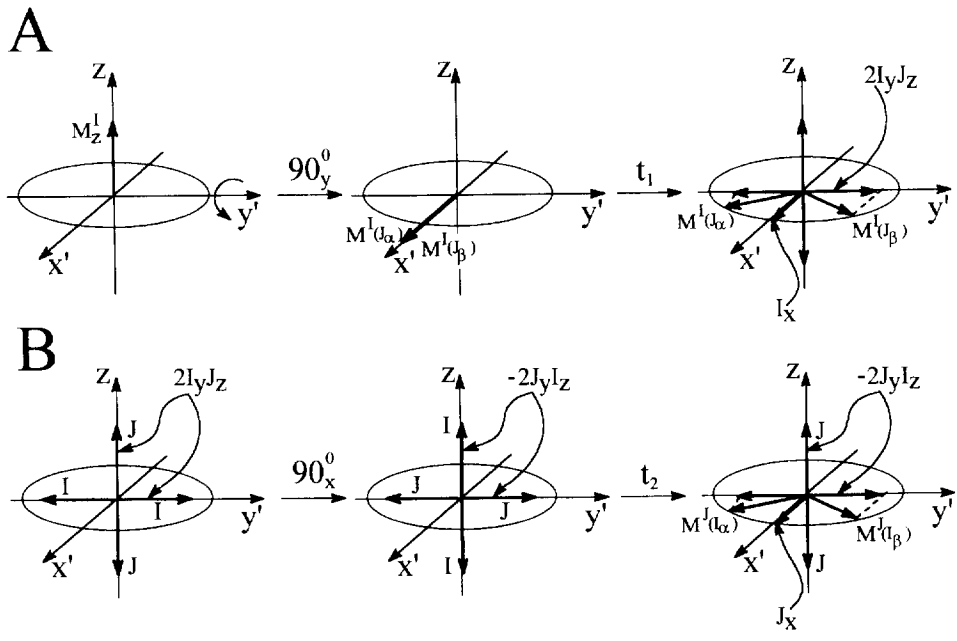

Fig. 7.14. Vector representation of a COSY experiment. The first 90° pulse along y' rotates the equilibrium magnetization of the I and J spins from the z axis to the x' axis. During t_1, the transverse doublet components of, e.g., signal I (assumed to precess at the rotating, frame frequency) separate. Their x' projections are in phase, while their y' projections are in antiphase. Antiphase magnetization is associated with the two opposite components of the J spin (hence the label $2I_yJ_z$ for the resulting four-vector pattern). The second 90° pulse along x' interchanges the I and J spins, producing a $-2J_xI_z$ antiphase product operator. During t_2 the latter generates a detectable in-phase magnetization of the J spin, whose initial intensity had been modulated by the I spin Larmor frequency during t_1, thus originating a cross peak.

neighbors have opposite M_z components (α *and* β). The projections of the two I components on the rotating frame axis on which the magnetization was tilted by the first 90° pulse (e.g. the x' axis) oscillate in phase (Fig. 7.14(A)) while those on the y' axis oscillate in antiphase. The in-phase and antiphase projections are also called single quantum and antiphase coherences. In the product operator language they are indicated as I_x and $2I_yJ_z$ (see Appendix V). The two are cyclically interconverted into one another during the time t_1. The antiphase coherence has indeed a strict 1:1 relationship with the corresponding two M_z components of the J spin (Fig. 7.14(A)).

When the second 90° pulse is applied, the antiphase magnetization of the I and J spins is interchanged (Fig. 7.14(B)). During t_2, the new antiphase coherence, $-2J_yI_z$, is again cyclically converted into a single quantum coherence J_x, which is a detectable magnetization of the J spin. The mixing formally occurs with the second 90°, and we have seen that the appropriate coherences must develop during both t_1 and t_2. If it were not for transverse relaxation, the antiphase coherence of the I spin would develop during t_1 proportionally to $\sin(\pi J_{IJ}t_1)$, and the maximal antiphase intensity would be obtained for $t_1 = 1/2J_{IJ}$. This sinusoidal dependence is, however,

damped by a term $\exp(-t_1/T_2^I)$. An analogous behavior is shown by the build up of the single quantum coherence J_x during t_2. Overall, the intensity of the cross peak builds up and decays according to the following relationship:

$$I(t) = \sin(\pi J_{IJ} t_1) \exp(-\rho_2^I t_1) \sin(\pi J_{IJ} t_2) \exp(-\rho_2^J t_2) \tag{7.2}$$

The two cross peaks are distinguished according to which of the two T_2^I or T_2^J constants appears in each dimension. From Eq. (7.2), it appears that the maximum information is not contained in the first data points. For $T_2 \gg 1/2J_{IJ}$, it is well known that the maximal intensity is obtained when the center of the t_1 and t_2 intervals is at $1/2J_{IJ}$, i.e. for $t_1^{max} = t_2^{max} = 1/J_{IJ}$. For $T_2 \ll 1/2J_{IJ}$, maximal intensity is obtained for $t_1^{max} = 2T_2^I$ and $t_2^{max} = 2T_2^J$. Of course, at these short time values, the sine build up of the interaction is small. Weighting functions of sin, $\sin^2$ or matched-filter-type are used to maximize the signal to noise ratio. In any case, since the T_2 values in paramagnetic compounds are small, the cross peak intensity is drastically reduced.

The coherence transfer provides cross peaks which are antiphase for the various J_{IJ}-split components. The antiphase nature of the cross peaks then leads to partial or total cancellation of the cross peaks themselves, especially if they are phased in the absorption mode. This behavior can be simulated (Fig. 7.15) using appropriate treatments of the time evolution of the spin system, for instance using the density matrix formalism (Appendix V). It is quite common that signals in paramagnetic systems are so broad as to wipe out the J_{IJ} splitting. It has been pointed out that, if the cross peaks are phased in dispersion mode rather than in absorption mode, the loss of intensity is drastically reduced [15]. Accurate phasing may be difficult, however, when the cross peak intensity is small, as happens in paramagnetic compounds. Acquisition and Fourier transform in the so called magnitude mode gives results that are of comparable quality but are absolutely insensitive to phasing. Indeed, in magnitude mode the intensity is given by

$$I = (A^2 + D^2)^{1/2} \tag{7.3}$$

where A and D stand for the pure absorption (or real) and pure dispersion (or imaginary) components of the signal respectively. In Fig. 7.16(A) part of the magnitude COSY spectrum of the pseudotetrahedral complex NiSAL–i-prop (scheme in the inset) is reported [16]. COSY cross peaks are evident between adjacent protons in the aromatic ring. Although the lines in this case are not very broad, it appears that the phase-sensitive spectrum, routinely phased in absorption mode, has a higher resolution than the magnitude mode spectrum but is of lower quality (Figs. 7.16(A) and 7.16(B)). A better quality is obtained by phasing the spectrum in dispersion mode (Fig. 7.16(C)). A good quality spectrum is also obtained with the in-phase

Fig. 7.15. Calculated shapes of cross peaks in COSY spectra characterized by $T_2 \ll 1/2J$ (conditions: $J = 8$ Hz; $T_2 = 5$ ms; $t_1^{max} = t_2^{max} = 10$ ms). (A) Phase-sensitive spectra, phased in dispersion mode; (B) phase-sensitive spectra, phased in absorption mode; (C) magnitude mode spectra. $\sin^2$ weighting functions are used.

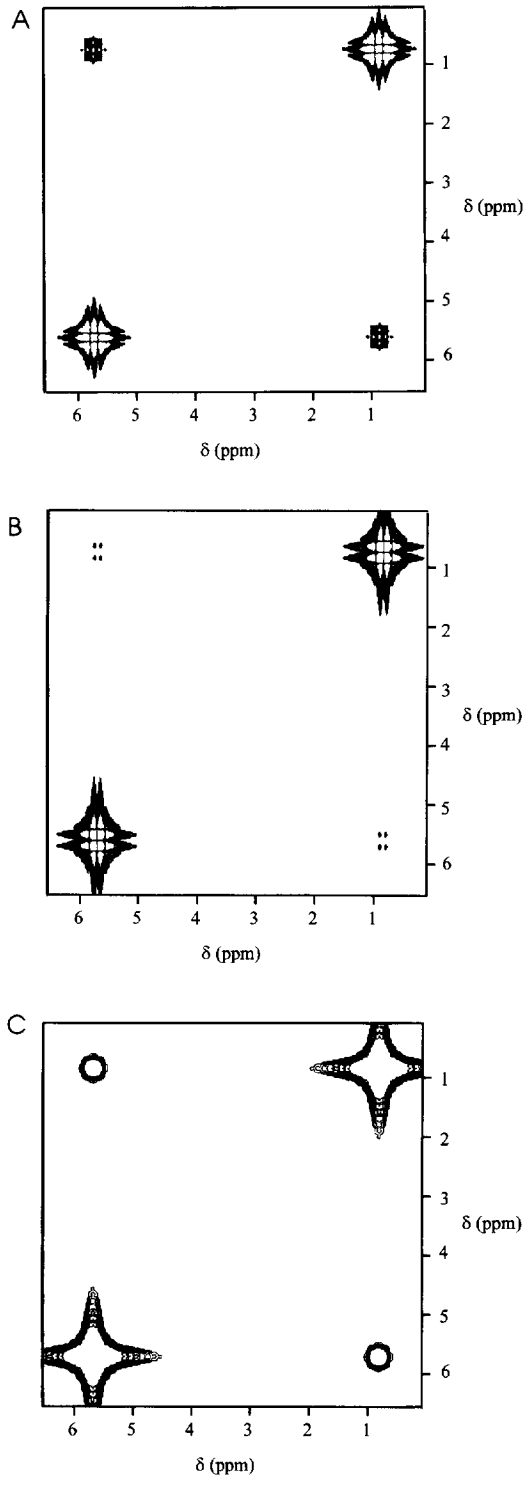
A
B
C
δ (ppm)
δ (ppm)
1
2
3
4
5
6
6
5
4
3
2
1

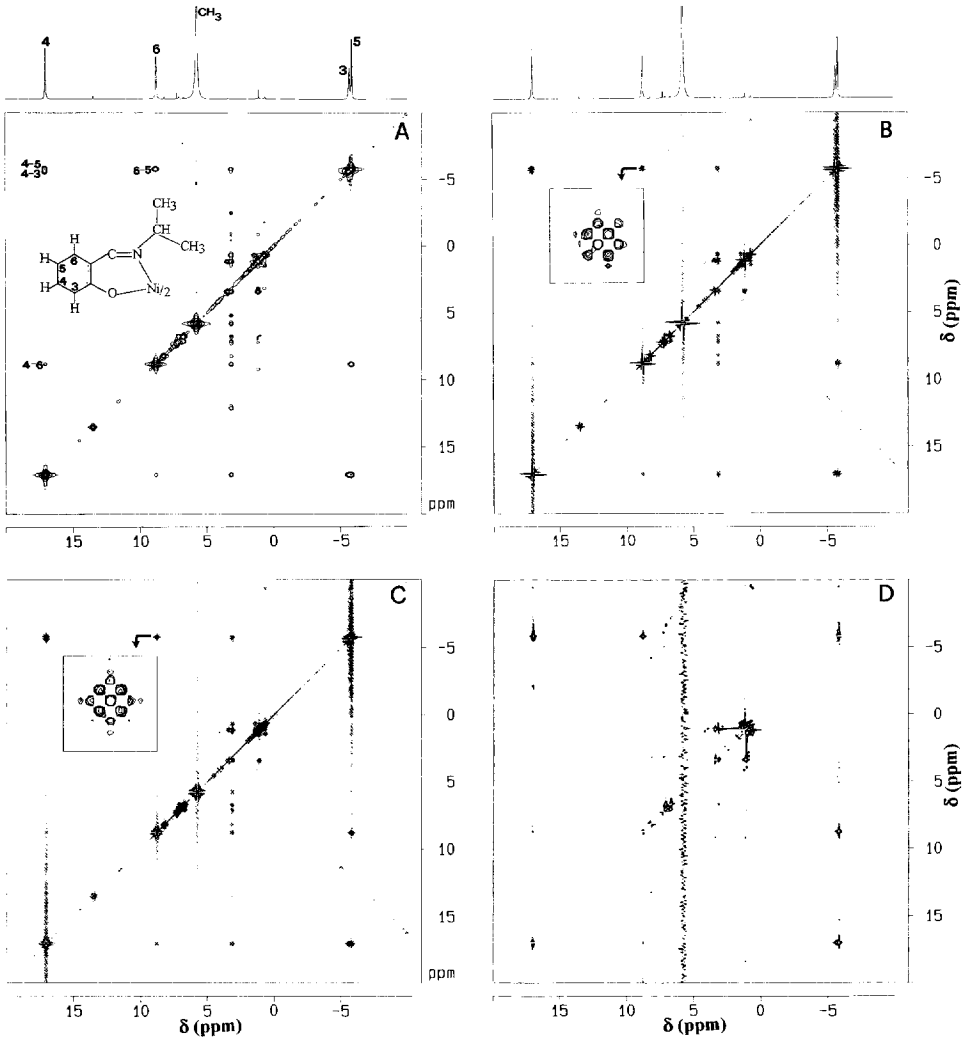

Fig. 7.16. Aromatic ring part of the COSY spectra of the complex shown in the inset [16]. (A) Magnitude mode spectrum; (B) phase-sensitive spectrum, absorption mode; (C) phase-sensitive spectrum, dispersion mode; (D) ISECR [17] spectrum (sequence in Fig. 7.2(D)). Sin^2 weighting functions have been used for spectra (A)–(C) and a cos^2 weighting function for spectrum (D). Peaks in (A) and (D) are in phase and positive. The positive components of the 6–5 peak in (B) and (C) are shown in the enlargements.

cross peaks COSY (ISECR COSY) sequence shown in Fig. 7.2D [17], which provides good resolution and in-phase cross peaks (Fig. 7.16(D)).

In macromolecular paramagnetic systems, further phenomena may concur which provide COSY cross peaks, when using the sequence of Fig. 7.2(C), whose nature is actually dipolar (see Section 7.8).

In several kinds of correlation spectroscopy it is customary to also exploit the evolution of either zero quantum (ZQ) or double quantum (DQ) coherences. As shown in Fig. 6.1, they correspond to the transition $-+ \rightarrow +-$ and $-- \rightarrow ++$ respectively. The typical pulse sequence is described in Fig. 7.2(E), where after the first 90° pulse we wait for a time $t_d/2$, then we send a 180° pulse which has the only role of refocusing the spins to avoid loss of in-plane magnetization due to magnetic field inhomogeneity. After the same time $t_d/2$ we send a 45° pulse in order to dislocate the antiphase coherence out of the yz plane in such a way as to create ZQ and DQ coherences (Fig. 7.2(E)). In the product operator formalism, DQ and ZQ coherences are proportional to $I_xJ_y \pm I_yJ_x$ respectively. I_yJ_x can be visualized as shown in Fig. 7.17. The time t_d should be optimized to either $1/2J_{IJ}$ or T_2. The DQ (ZQ) coherence is let evolve for a time t_1. At this point we can apply a 90° pulse to transform back into an antiphase coherence either the DQ or the ZQ coherence depending on the phase cycling (Fig. 7.17).

Since there is a waste of time in the phase cycling (and some extra loss of signal due to the overall length of the sequence), there is no advantage in using these or other COSY techniques in the place of the simple COSY experiment described in Fig. 7.2(C). However, the relaxation of the ZQ transitions may be little affected by

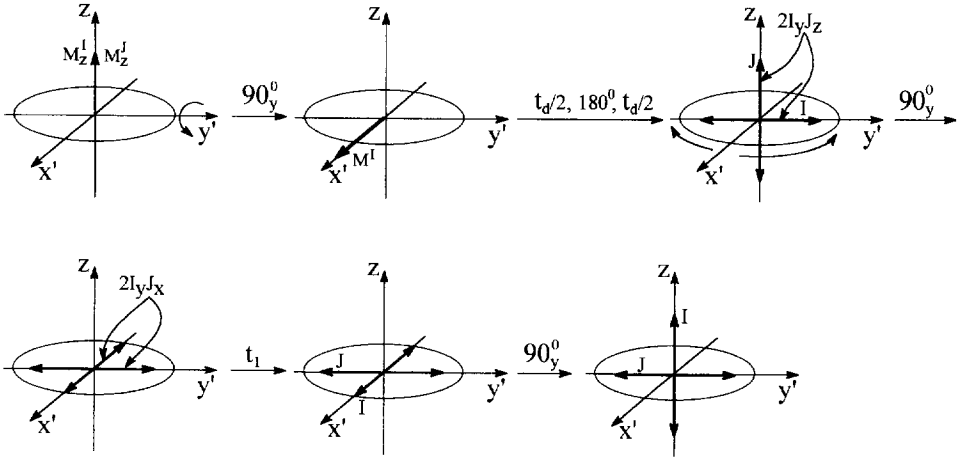

Fig. 7.17. Vector representation of a DQ (ZQ) experiment. The first 90° pulse along y' rotates the equilibrium magnetization of the I (and J) spins from the z axis to the x' axis. After a time $t_d = 1/2J_{IJ}$ (interrupted by a refocusing 180° pulse), the antiphase coherence $2I_yI_z$ is at its maximum. Another pulse along y' (shown as a 90° pulse for clarity, although 45° pulses are more commonly used) then transforms the antiphase coherence into a DQ (ZQ) coherence (the $2I_yJ_x$ component is shown). During t_1 the DQ (ZQ) evolves until a further 90° pulse along y' transforms the $-2I_xJ_y$ component (shown at its maximum for clarity) into a $2J_yI_z$ antiphase coherence. During t_2 the latter generates a detectable in-phase magnetization of the J spin, whose initial intensity had been modulated by the DQ (ZQ) Larmor precession frequency during t_1, thus originating a cross peak.

the presence of unpaired electrons and under certain conditions may also have some advantages as far as resolution is concerned [18].

7.6. The TOCSY experiment

TOCSY is a rotating frame experiment designed to detect scalar connectivities over a large range of J_{IJ} values, especially useful for small (ca. 1 Hz) J_{IJ} values. The most common pulse sequence is shown in Fig. 7.2(F) [19]. The spin lock is achieved by applying a train of relatively high power pulses (the MLEV17 sequence being one of the most used sequences [20]) in such a way as to continuously refocus the chemical shift evolution of the various signals in the xy plane. Analogously to ROESY experiments, the magnetization during the spin lock (mixing) time disappears with $T_{1\rho}$ (i.e. essentially T_2, see Section 3.4). It follows that coherence transfer in the xy plane, which is built up with a $\sin(\pi J_{IJ}t)$ function, also decreases with time constant $\rho_{1\rho} = (\rho^I_{1\rho} + \rho^J_{1\rho})/2$:

$$I = \sin(\pi J_{IJ} t_m) \exp(-\rho_{1\rho} t_m) \tag{7.4}$$

A TOCSY experiment on a paramagnetic molecule is reported in Fig. 7.7 for the 5Cl–Ni–SAL–MeDPT complex [5]. Cross peaks between signals with linewidths of the order of 100 Hz were easily detected. In particular, the couplings of each aromatic proton with its neighbors are evident. TOCSY cross peaks between signals with similarly broad lines can also be detected in proteins (see Fig. 7.18) [21].

In TOCSY experiments, the problem of overheating the sample is more serious than in ROESY experiments because of the large irradiation energy required by the spin lock pulse. Each individual component of the pulse train must have enough power to irradiate the whole spectral window of interest. Spin-lock sequences different from the MLEV17 sequence, that may alleviate the heating problem, are discussed in Section 9.4.2. Other modifications that are useful to eliminate unwanted NOESY cross peaks from TOCSY spectra can also be found in Section 9.4.2.

7.7. Heterocorrelation spectroscopy

2D spectra are in principle possible for heteronuclei coupled by either dipolar or scalar interactions. However, the magnetic moments of heteronuclei are sizably smaller than that of the proton, and since cross relaxation depends on the square of the magnetic moment it appears that this is a serious limitation for the observation of NOESY or ROESY cross peaks. However, as already discussed, in scalar-coupled systems the relevant coherences build up with $\sin(\pi J_{IJ}t)$. Since J_{IJ} in $^{13}C^1H$ and $^{15}N^1H$ moieties is of the order of 10^2 Hz, as opposed to about 10 Hz between proton pairs, it is conceivable that scalar correlation experiments are successful. Heterocorrelated spectra have the advantage of allowing one to detect signals of protons attached to carbons or nitrogens when they are within a crowded envelope.

Heterocorrelations can be detected both in direct and reverse modes. In the latter

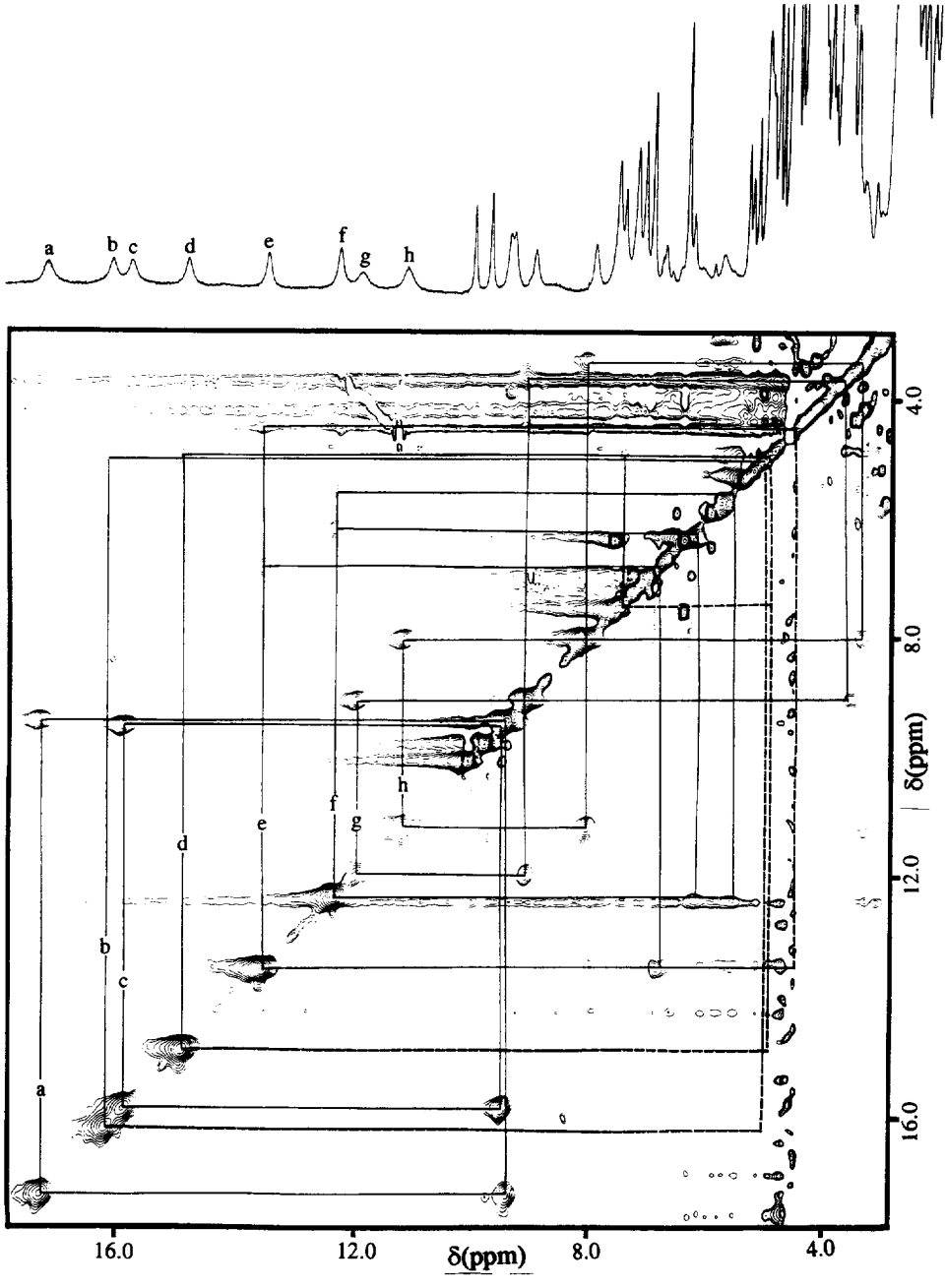

Fig. 7.18. TOCSY spectrum of the oxidized form of ferredoxin from *C. pasteurianum*, showing all the cysteine ligand β-CH_2–β-CH_2 and some β-CH_2–α-CH connections [21].

mode, dramatic enhancements of sensitivity can be achieved owing to the larger sensitivity of protons with respect to heteronuclei. In the most common heterocorrelation pulse sequences for reverse detection, called heteronuclear multiple quantum correlations (HMQC) (Fig. 7.2(G)) [22,24], ^{1}H–^{13}C DQ coherence is generated by first applying a 90° pulse on protons and, after a time t_d chosen equal to $1/2J_{IJ}$, by applying a 90° pulse on carbon (Fig. 7.19). At this point the DQ coherence is let evolve for a variable time t_1. Often, a refocusing 180° pulse on proton is applied at $t_1/2$. A further 90° pulse on carbon converts the DQ coherence into an antiphase magnetization (Fig. 7.19), which is let evolve for another time t_d to fully develop the observable single quantum coherence on proton, which is then detected during the acquisition time t_2.

In paramagnetic compounds, in the absence of contact relaxation, heteronuclei are relaxed much less than protons by dipolar coupling with the unpaired electron(s), all other things being equal, because of the γ_I^2 dependence. By looking at the magnetization behavior during the experiment, we can predict the relaxation of the system during the sequence. When the linewidths are larger than J_{IJ}, the first antiphase on proton decays during t_d essentially with ρ_2^I for proton (the heteronucleus being still along the z axis). The DQ (or ZQ) decays with the sum of $\rho_2^I + \rho_2^J$, whereas during the second t_d the magnetization decays again with ρ_2^I. In cases where $\rho_2^I \gg \rho_2^J$ (for instance, large Curie relaxation effects on protons, see Section 3.6), direct detection may be less disfavored than reverse detection, because during the two t_d intervals ρ_2^J instead of ρ_2^I is involved. The effects, however, are seldomly so large as to make direct detection more convenient.

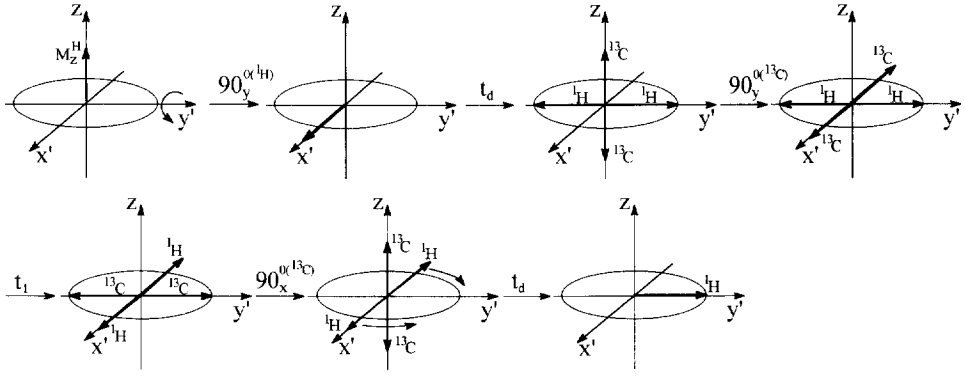

Fig. 7.19. Vector representation of a ^{1}H–^{13}C HMQC experiment. The first 90° pulse along y' rotates the equilibrium magnetization of the proton spin, I^H, from the z axis to the x' axis. After a time $t_d = 1/2J_{HX}$, the antiphase coherence $2I_y^H I_z^C$ is at its maximum. A 90° pulse on carbon along y' then transforms the antiphase coherence into a DQ (ZQ) coherence (the $2I_y^H I_x^C$ component is shown). During t_1 the DQ (ZQ) evolves (with a 180° refocusing pulse on proton in the middle), until a further 90° pulse on carbon along x' transforms the $-2I_x^H I_y^C$ component (shown at its maximum for clarity) into a $2I_x^H I_z^C$ antiphase coherence. After the time t_d, in-phase magnetization of the proton spin develops. The latter is detected during t_2. Its initial intensity is modulated by the carbon Larmor frequency during t_1 (if proton refocusing has been used), thus originating a proton–carbon cross peak.

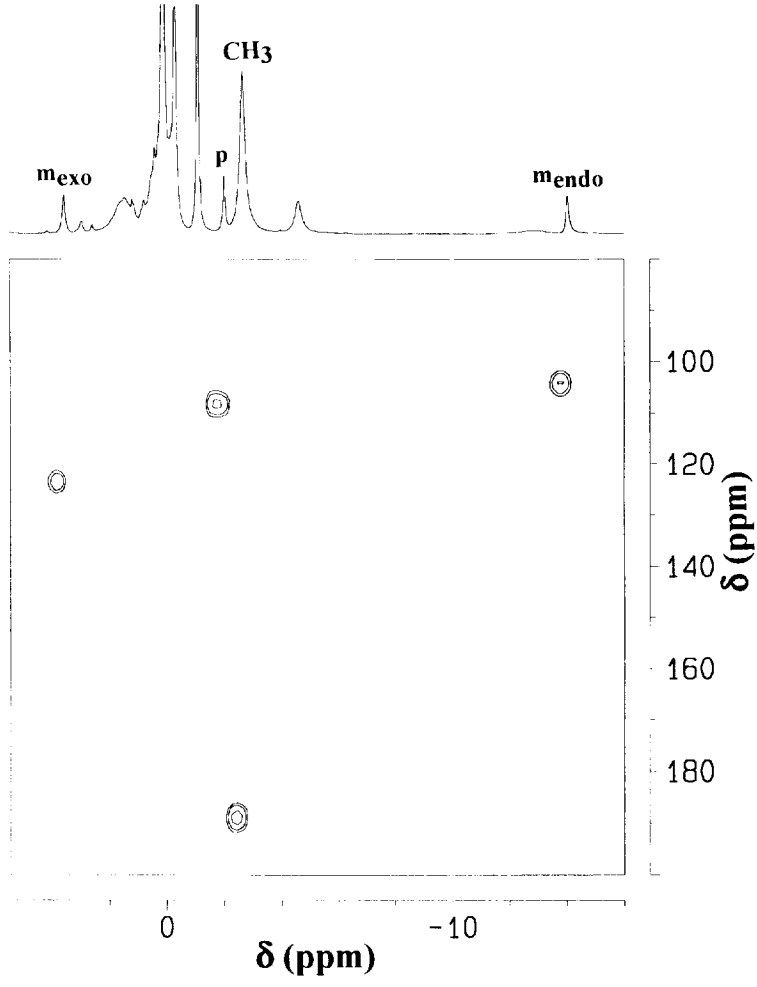

Fig. 7.20. 600 MHz natural abundance ^{1}H—^{13}C reverse HMQC spectrum of the complex shown in Fig. 7.13 (Ln = Pr^{3+}). The cross peaks involve protons with linewidths of the order of, or larger than, J_{HC} [18].

An example of an HMQC spectrum is reported in Fig. 7.20 [18]. ^{1}H–^{13}C connectivities can be detected for signals for which $T_2 < 1/2J_{IJ}$ by setting $t_d = T_2$.

7.8. Coherence transfer caused by dipolar cross correlation

When reference was made to the dipolar coupling scheme between two protons of Fig. 6.1, it was implicitly assumed that the two single quantum longitudinal transition probabilities of, for instance, nucleus I, w_1^I, were equal, i.e. that they were independent of the spin state of nucleus J. Similar assumptions are made when

dealing with transverse transition probabilities. When the coupling is dipolar in origin, the two transitions are degenerate. Indeed, one never thinks of a signal belonging to a nucleus dipole-coupled to another nucleus as resulting from the superposition of two coincident components with equal T_1 and T_2. There are a number of cases of dipole-coupled pairs, however, where the two components, still coincident due to the absence of scalar couplings, have different T_1 and T_2. This phenomenon originates from cross correlation between the dipolar coupling operative within the pair and other interactions experienced by the two nuclei and modulated by the same motion responsible for the modulation of the dipolar coupling [25]. In principle, a third nuclear spin K dipole-coupled to the other two spins I and J is sufficient to differentiate the linewidths. In practice, the effect is small and hardly detectable. A more efficient mechanism is the cross correlation with the chemical shift anisotropy relaxation mechanism.

In paramagnetic systems, a major nuclear relaxation mechanism is Curie relaxation (see Section 3.6). In paramagnetic macromolecules Curie spin relaxation is often the dominant contribution to T_2. It has been recently discovered [26] that cross correlation between proton–proton dipolar coupling and Curie relaxation may cause the two degenerate signal components of each nucleus to have markedly different linewidths. Under these conditions, the common COSY experiment of Fig. 7.2(C) yields strong cross peaks between signals coupled by dipolar *but not by scalar* interactions. The origin of the phenomenon can be better understood if one recalls that the components of COSY cross peaks are in antiphase (see, for instance, Figs. 7.16(B) and 7.16(C)). It is obvious that, if the two components coincide, total cancellation occurs. However, if the two components have different linewidths, they do not cancel and may give rise to very strong cross peaks, as illustrated in Fig. 7.21.

7.9. Beyond 2D spectroscopy

In a chapter regarding 2D NMR spectroscopy of paramagnetic molecules, the obvious perspective is that of using three-dimensional (3D) NMR for paramagnetic molecules. The demand for 3D spectroscopy is based on a need of increased resolution when macromolecules are concerned. It is possible that for small complexes 3D spectroscopy will never be necessary. However, everytime something new has appeared in science, the majority has reacted by saying that the utility was scarce in their own field, and the majority has not always been right. Therefore, we do not commit ourselves.

We have seen in Section 7.3 that one limitation of 2D spectroscopy when dealing with paramagnetic compounds showing a wide range of T_1 (and T_2) values is that the parameters cannot be optimized for the detection of all connectivities in a single experiment. Often, at least two experiments are necessary. An advantage of 3D spectroscopy which is peculiar to paramagnetic systems, and in particular to paramagnetic macromolecules, is that one can cover the whole range of T_1 and T_2 values present in the spectrum by optimizing the spectral parameters in one 2D plane (spectral resolution, maximal evolution time, mixing time, etc.) to the detection of

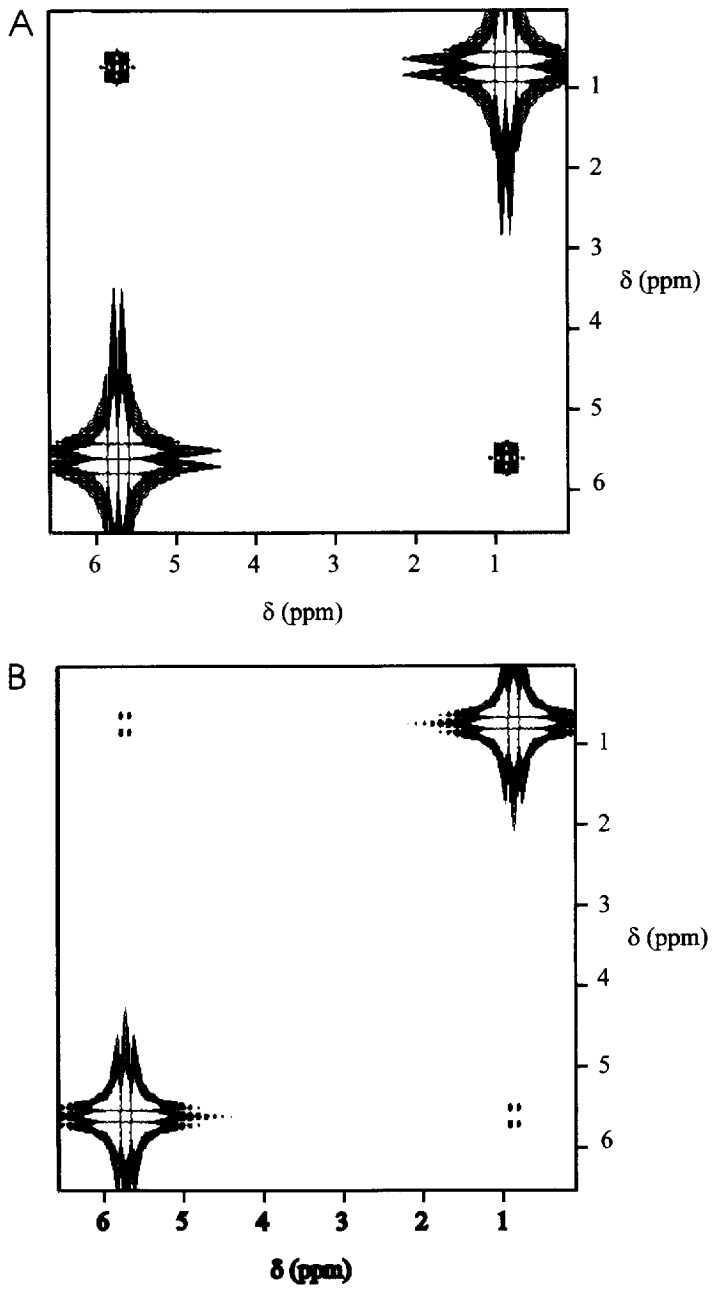

Fig. 7.21. Simulated COSY cross peaks originating from a pair of signals dipole-coupled in the presence of cross relaxation with Curie relaxation and in the absence of scalar coupling. The two degenerate components are in antiphase, but they do not cancel out due to their different linewidths. Note that absorption mode phasing (A) and dispersion mode phasing (B) show opposite patterns with respect to the case of scalar coupling (Figs. 7.15(A) and 7.15(B)).

connectivities between fast relaxing signals, and those in another 2D plane to the detection of connectivities with slow relaxing signals. Of course, a clear advantage only appears when fast relaxing signals are many and severely overlapped with slow relaxing signals.

An obvious extension to 3D spectroscopy from 2D spectroscopy is the homonuclear NOESY–NOESY [27]. There are two t_1 variable times and one t_2, which after Fourier transform provide three frequency domains. The 3D NOESY–NOESY spectrum of met-myoglobin cyanide, which contains low spin iron(III) in a heme moiety (see Fig. 2.14), has been successfully measured [28]. In Fig. 7.22 a slice of the 3D spectrum is shown at the 12-CH_3 height. On the diagonal it shows all the

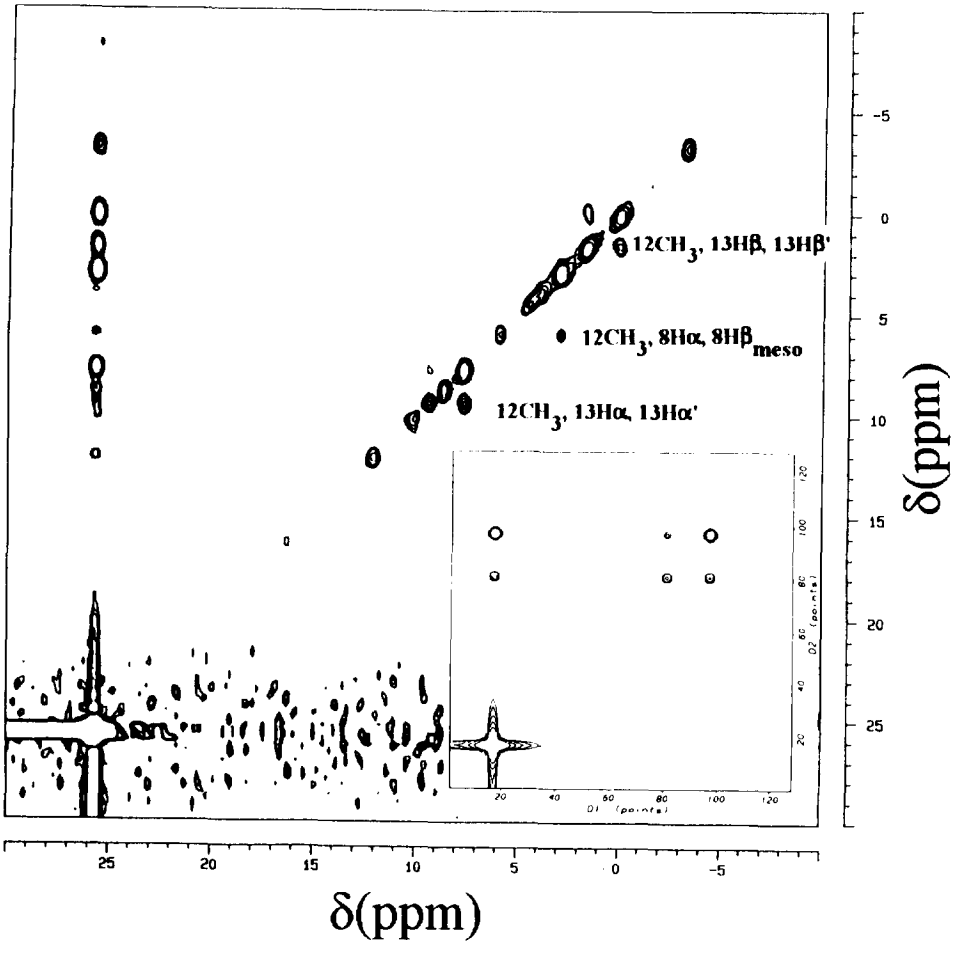

Fig. 7.22. Cross-section of the 600 MHz 3D NOESY–NOESY spectrum of met-myoglobin cyanide. The slice is taken at the 12-CH_3 height. The inset shows the simulated cross-section involving the 12-CH_3, 13-Hα and 13-Hα′ signals [28].

dipolar connectivities between 12-CH_3 and other protons; off-diagonal there are dipolar connectivities within the latter set of protons, all belonging to the porphyrin ring.

Results similar to those shown in the slice of Fig. 7.22 can be obtained with the so-called NOE–NOESY sequence [29]. Here a hyperfine shifted signal, e.g. 12-CH_3 of the above compound, is selectively saturated, and then the NOESY pulse sequence is applied. The NOESY difference spectrum obtained by subtracting a NOESY spectrum without presaturation of the 12-CH_3 signal is shown in Fig. 7.23. Here, some more cross peaks are evident with respect to the 3D NOESY–NOESY experiment because secondary NOEs develop much more when the primary NOEs from the 12-CH_3 signal evolve in a steady state experiment like the NOE–NOESY rather than in a transient-type experiment like the NOESY–NOESY. In Fig. 7.23, dipolar connectivity patterns are apparent among protons belonging to Phe-33 (2) Phe-43 (1, 6, 7, 8), Phe-46 (3) and propionate 13 (9, 10). Some of these assignments could only be performed by exploiting the NOE–NOESY experiment.

Other variants are NOE–COSY and NOE–TOCSY. However, these experiments are much less sensitive than NOE–NOESY.

Sometimes it may be useful to suppress signals with long relaxation times in such a way as to detect cross peaks involving one fast relaxing signal under the envelope of diamagnetic signals. In this case a SuperWEFT sequence (180–τ–90–AQ, see Section 9.1.2) is applied before performing the 2D experiment. By appropriately choosing the τ value, the diamagnetic signals can be brought to have intensities close to zero.

In principle, all the combinations of homonuclear 2D spectroscopies can be performed to originate a 3D spectrum (COSY–COSY, NOESY–COSY, NOESY–TOCSY, etc.). The considerations made in this chapter for the most basic experiments can be easily extended to their combinations. The general guideline should always be that the more complex the pulse sequence is, the more the experimental sensitivity will suffer from fast nuclear relaxation.

The most useful advantage of 3D spectroscopy, however, is that heteronuclei can be included along one dimension. If one of the two 2D sequences is a Hetcor sequence, then simultaneous heteronucleus–proton connectivities can be observed. In the case of macromolecules, where there are solubility problems, heteronuclear enrichment is probably required[1].

7.10. Towards the solution of tridimensional structures in solution

NOEs or NOESY cross peaks can be used to define distances between protons. When appropriate, the hyperfine shifts may also contain information on the

[1] **Note added in proof.** Sophisticated Hetcor spectroscopies, of the type of those used in diamagnetic systems, have been recently performed with success on a paramagnetic protein containing the $[Fe_4S_4]^{2+}$ polymetallic center (I. Bertini, M.M.J. Couture, A. Donaire, L.D. Eltis, I.C. Felli, C. Luchinat, M. Piccioli and A. Rosato, Eur. J. Biochem., in press).

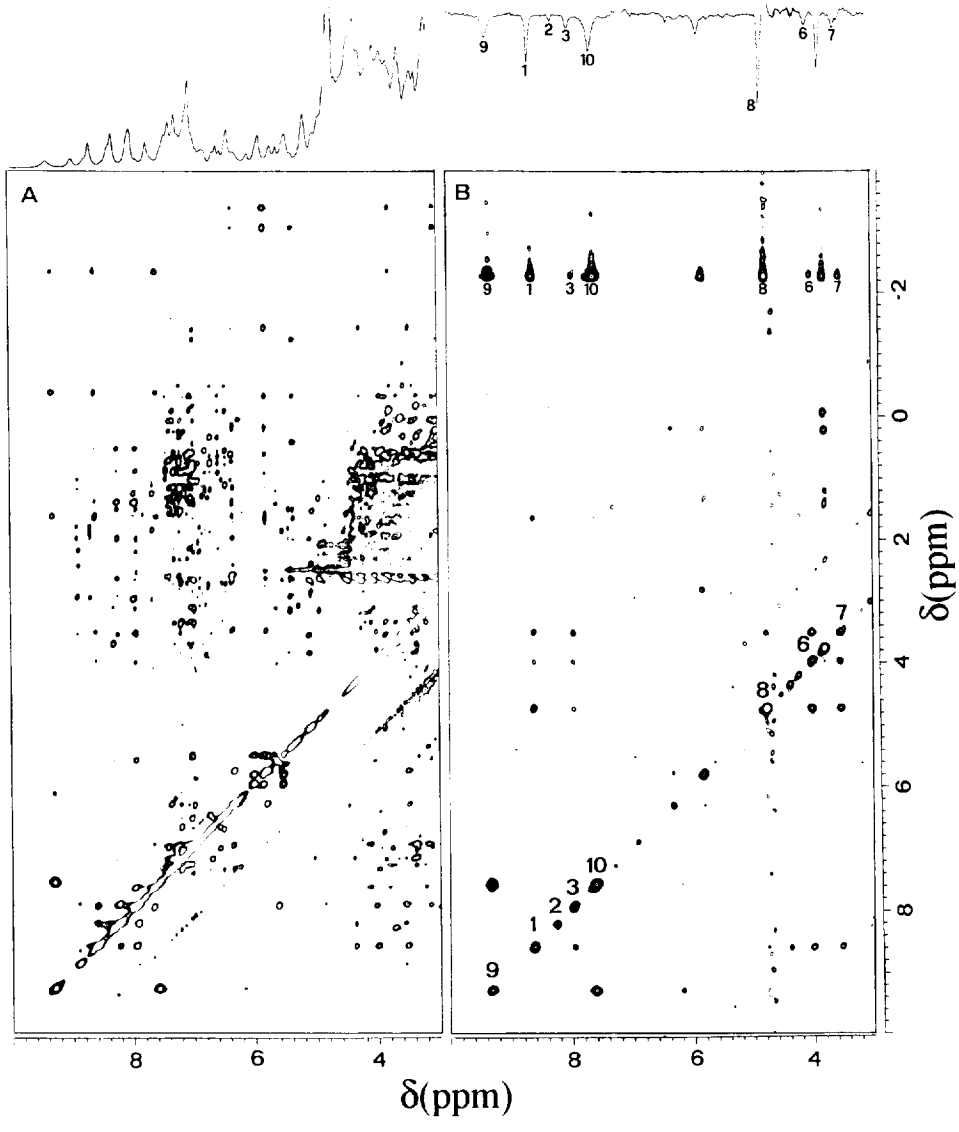

Fig. 7.23. NOESY spectrum (A) and NOE–NOESY spectrum (B) of met-myoglobin cyanide [29]. The latter spectrum is obtained by pre-irradiation of the 12-CH_3 signal.

metal–donor–C–H or C–C dihedral angles as discussed in Section 2.4. Organic chemists know well that the three-bond scalar coupling constants $3J_{IJ}$ between nuclei I and J obey a relationship of the type [30]

$$^3J_{IJ} = a\cos^2\theta + b\cos\theta + c \tag{7.5}$$

where θ is the I–X–Y–J dihedral angle. When I and J are protons, the problem

arises of detecting splitting or COSY cross peak components in the case of hyperfine broadened signals. Some sequences known as E. COSY [31] or ZQ/DQ-COSY are designed to detect small J_{IJ} values where three or more atoms separate two protons, or a proton and a heteronucleus. At this moment the limits of these techniques in paramagnetic molecules are being tested.

The problem is now that of having enough structural information, i.e. experimental structural constraints, to provide an accurate structural model. In proteins, the folding permits the detection of a number of NOEs such that the solution structure can be achieved [32,33]. With the advancement of theory and practice, the solution structure of paramagnetic metalloproteins can be achieved if the electronic relaxation times are favorable [34–37]. In this case, to the usual NOE and ^3J constraints, those contained in the hyperfine coupling can be added, i.e. the pseudocontact shifts which are dipolar in nature [38] and T_{1M}^{-1} when the dipolar contribution is dominant [39]. It is possible that in small coordination compounds where the number of NOEs is necessarily small, the combination of the various constraints provides a reasonably well-defined average structure in solution. This route has not been pursued much in the literature. Less dramatic than in small coordination compounds, but quite serious, is the problem of DNA/RNA fragments. Early successes were obtained with mononucleotides [40,41]. In oligonucleotides, the signal overlap is severe and the folding is such that the number of NOEs is small. Many J values are needed, which can be obtained only by using fully isotope-labeled samples [42]. If a binding site were available for a paramagnetic metal ion, the induced pseudocontact shifts and nuclear relaxation enhancements could be of significant help.

References

[1] H. Santos, D.L. Turner, A.V. Xavier and J. LeGall, J. Magn. Reson., 59 (1984) 177.
[2] W. Peters, M. Fuchs, H. Sicius and W. Kuchen, Angew. Chem., 24 (1985) 231.
[3] B.G. Jenkins and R.B. Lauffer, Inorg. Chem., 27 (1988) 4730.
[4] B.G. Jenkins and R.B. Lauffer, J. Magn. Reson., 80 (1988) 328.
[5] C. Luchinat, S. Steuernagel and P. Turano, Inorg. Chem., 29 (1990) 4351.
[6] I. Bertini, F. Briganti, C. Luchinat, L. Messori, R. Monnanni, A. Scozzafava and G. Vallini, Eur. J. Biochem., 204 (1992) 831.
[7] H. Kessler, H. Oschkinat, C. Griesinger and W. Bermel, J. Magn. Reson., 70 (1986) 106.
[8] I. Bertini, L. Sacconi and G.P. Speroni, Inorg. Chem., 11 (1972) 1323.
[9] C. Luchinat and M. Piccioli, in G.N. La Mar (Ed), NMR of Paramagnetic Macromolecules, NATO ASI Series, Kluwer Academic, Dordrecht, 1995, pp. 1–28.
[10] I. Bertini, F. Briganti, C. Luchinat, L. Messori, R. Monnanni, A. Scozzafava and G. Vallini, FEBS Lett., 289 (1991) 253.
[11] K. Nagayama, A. Kumar, K. Wüthrich and R.R. Ernst, J. Magn. Reson., 40 (1980) 321.
[12] I. Bertini, C. Luchinat, L. Messori and M. Vasak, Eur. J. Biochem., 211 (1993) 235.
[13] C.A. Salgueiro, D.L. Turner, H. Santos, J. LeGall and A.V. Xavier, FEBS Lett., 314 (1992) 155.
[14] I. Bertini, A. Coutsolelos, A. Dikiy, C. Luchinat, G. Spyroulias and A. Troganis, Inorg. Chem., in press.
[15] A.V. Xavier, D.L. Turner and H. Santos, Methods Enymol., 227 (1993) 1.
[16] I. Bertini and C. Luchinat, unpublished results, 1996.
[17] S. Talluri and H.A. Scheraga, J. Magn. Reson., 86 (1990) 1.

[18] I. Bertini, C. Luchinat and A. Rosato, Chem. Phys. Lett., 250 (1996) 495.
[19] L. Braunschweiler and R.R. Ernst, J. Magn. Reson., 53 (1983) 521.
[20] A. Bax and D.G. Davis, J. Magn. Reson., 65 (1985) 355.
[21] M. Sadek, R.T.C. Brownlee, S.D.B. Scrofani and A.G. Wedd, J. Magn. Reson. B, 101 (1993) 309.
[22] L. Müller, J. Am. Chem. Soc., 101 (1979) 4481.
[23] A. Bax, R.H. Griffey and B.L. Hawkins, J. Am. Chem. Soc., 105 (1983) 7188.
[24] A. Bax, R.H. Griffey and B.L. Hawkins, J. Magn. Reson., 55 (1983) 301.
[25] S. Wimperis and G. Bodenhausen, Mol. Phys., 66 (1989) 897.
[26] I. Bertini, C. Luchinat and D. Tarchi, Chem. Phys. Lett., 203 (1993) 445.
[27] R. Boelens, G.W. Vuister, T.M.G. Koning and R. Kaptein, J. Am. Chem. Soc., 111 (1989) 8525.
[28] L. Banci, W. Bermel, C. Luchinat, R. Pierattelli and D. Tarchi, Magn. Reson. Chem., 31 (1993) S3.
[29] I. Bertini, A. Dikiy, C. Luchinat, M. Piccioli and D. Tarchi, J. Magn. Reson Ser. B, 103 (1994) 278.
[30] M. Karplus, J. Chem. Phys., 30 (1959) 11; J. Am. Chem. Soc., 85 (1963) 2870.
[31] C. Griesinger, O.W. Sorensen and R.R. Ernst, J. Am. Chem. Soc., 107 (1985) 6394.
[32] G. Wagner, Progr. Nucl. Magn. Reson. Spectrosc., 22 (1990) 101.
[33] G.M. Clore and A.M. Gronenborn, Prog. Nucl. Magn. Reson. Spectrosc., 23 (1991) 43.
[34] L. Banci, I. Bertini, L.D. Eltis, I.C. Felli, D.H.W. Kastrau, C. Luchinat, M. Piccioli, R. Pierattelli and M. Smith, Eur. J. Biochem., 225 (1994) 715.
[35] L. Banci and R. Pierattelli, in G.N. La Mar (Ed.), Nuclear Magnetic Resonance of Paramagnetic Macromolecules. NATO ASI Series, Kluwer Academic, Dordrecht, 1995, pp. 281–296.
[36] I. Bertini, A. Dikiy, D.H.W. Kastrau, C. Luchinat and P. Sompornpisut, Biochemistry, 34 (1995) 9851.
[37] I. Bertini, A. Donaire, B.A. Feinberg, C. Luchinat, M. Piccioli and H. Yuan, Eur. J. Biochem., 232 (1995) 192.
[38] L. Banci, I. Bertini, K.L. Bren, M.A. Cremonini, H.B. Gray, C. Luchinat and P. Turano, JBIC, 1 (1996) 117.
[39] I. Bertini, A. Donaire, C. Luchinat and A. Rosato, submitted.
[40] C.D. Barry, A.C.T. North, J.A. Glasel, R.J.P. Williams and A.V. Xavier, Nature, 232 (1971) 236.
[41] C.D. Barry, J.A. Glasel, R.J.P. Williams and A.V. Xavier, J. Mol. Biol., 84 (1974) 471; J. Mol. Biol., 84 (1974) 491.
[42] J.P. Marino, H. Schwalbe, C. Anklin, W. Bermel, D.M. Crothers and C. Griesinger, J. Am. Chem. Soc., 116 (1994) 6472.

General references

A. Bax, Two Dimensional Nuclear Magnetic Resonance in Liquids, Reidel, Dordrecht, 1982.
R.R. Ernst, G. Bodenhausen and A. Wokaun, Principles of Nuclear Magnetic Resonance in One and Two Dimensions, Oxford University Press, London, 1987.